# Cold-dark-matter cosmology with non-Gaussian fluctuations from inflation

D. S. Salopek

*Department of Applied Mathematics and Theoretical Physics, Silver Street, Cambridge CB3 9EW, England
and NASA/Fermilab Astrophysics Center, P.O. Box 500 MS-209, Batavia, Illinois 60510*

Non-Gaussian primordial fluctuations for structure formation may be generated during the inflationary epoch from the nonlinear interaction of two scalar fields with gravity. Semianalytical stochastic inflation calculations are described for nonlinear long-wavelength evolution in $3+1$ dimensions. Long-wavelength fields are governed by a single equation, the separated Hamilton-Jacobi equation. Typically, non-Gaussian fluctuations arise when the scalar fields pass over a sharp feature in their potential surface. The subsequent evolution of these primordial fluctuations are calculated as scales reenter the horizon during the radiation-dominated and matter-dominated eras of the cold-dark-matter scenario. Contour maps for the linear density perturbation as well as the gravitational potential are displayed at the present epoch. In qualitative agreement with observations, one can construct models with enhanced sheetlike structures on the scale of $\sim 25 h^{-1}$ Mpc. The cleanest test of non-Gaussian fluctuations will hopefully occur in the near future from large-angle microwave-background anisotropy experiments.

## I. INTRODUCTION

With the decline of the simplest cold-dark-matter (CDM) scenario [1], it is imperative that theorists propose alternative models which can be compared with cosmological observations [2–6]. Here, I describe a variation of the inflation model which yields non-Gaussian primordial fluctuations. This model may be tested in the near future if the Cosmic Background Explorer (COBE) satellite [7] measures the microwave-background temperature anisotropy.

Even with the difficulties in accounting for large-scale structure in the Universe, it is still reasonable to retain the inflationary scenario. Redshifts of Infrared Astronomy Satellite (IRAS) galaxies [8] and their inferred peculiar velocities indicate that the Universe is at critical density [9,10] $\Omega = \rho/\rho_{\mathrm{crit}} = 0.8 \pm 0.3$. This result gives support to inflation whose most outstanding prediction was that $\Omega = 1$. However, one must attempt to modify or improve the scenario. For example, one may conjecture a set of primordial fluctuations that are richer than scale-invariant Gaussian fluctuations. I will describe a chaotic inflation model that gives non-Gaussian fluctuations which are basically scale invariant [11,12].

Non-Gaussian fluctuations for structure formation have been advocated by numerous researchers. Peebles [13,14] has suggested that the distribution of galaxies is not adequately described by a Gaussian process. Cosmic-string models [15] were among the first cosmological scenarios requiring non-Gaussian statistics. It has been shown recently that their signature is obscured by evolution of the string network [16], although it is possible that the initial conditions for cosmic strings are more complicated than originally anticipated [17]. Late-time phase transitions [18], extended inflation [19], and textures [20] are additional models whose statistics may not be described by a Gaussian distribution. In the context

of inflationary models, Allen, Grinstein, and Wise [21] were the first to construct axion models with non-Gaussian fluctuations [22]. Bardeen used two scalar fields to produce a "Gaussian-squared" model that had interesting cosmological consequences [23].

There are three essential ingredients to the inflationary scenario. Firstly, a scalar field with potential $V(\phi)$ models the decay of the cosmological constant. Secondly, gravity is crucial in order to account for the expansion of the Universe. Finally, scalar-field quantum fluctuations are necessary to produce inhomogeneities that will eventually produce structure in our Universe. One should view the inflation model as a microscope that magnifies quantum fluctuations at the smallest imaginable distance scales (less than the Planck length) to scales that are cosmologically observable. One of the problems with linear perturbation theory was that there was no short-distance cutoff. This gave the illusion that one could extrapolate to arbitrarily small distances. However, nonlinearities must be important at some scale.

Non-Gaussian fluctuations would be the signature of nonlinearities in the inflationary scenario. Their calculation is problematic because one requires a formalism that governs the evolution of quantum noise with gravity. Ideally, one needs a quantum theory of the gravitational field [24,25]. In order to bypass this very severe difficulty, I will use three tricks.

(1) Long-wavelength quantum noise behaves essentially classically, and it may be described using classical random fields in a process termed stochastic inflation [26–33]. Using the Wheeler-DeWitt equation, one may show that quantum gravity corrections are typically small [31].

(2) The classical nonlinear evolution of long-wavelength scalar fields and gravity is tractable [31,34]. When the wavelength of a fluctuation exceeds the Hubble radius, different spatial points are no longer in causal

contact, and they evolve as independent homogeneous universes. One may safely neglect second-order spatial gradients in the action for scalar fields and gravity. Nonetheless, one must carefully join the independent spatial points to make one Universe.

(3) The long-wavelength equations may be solved analytically when the logarithm of the scalar-field potential is linear [34]: $\ln V(\phi_j) = \sum_k a_k \phi_k$, where the $a_k$ are constants. More complicated potentials may be approximated by joining various linear $\ln V$ potentials together. In this way, one may produce models that yield non-Gaussian fluctuations that are consistent with current microwave-background anisotropy limits.

Originally, Ortolan, Lucchin, and Matarrese [35,36] had suggested that non-Gaussian fluctuations could arise from stochastic inflation if a single scalar field interacted through an exponential potential. However, using exact solutions of the improved Fokker-Planck equation, Salopek and Bond [32] showed that such scalar-field fluctuations were non-Gaussian only on scales much larger than our observable Universe (see also Refs. [37] and [38]). In addition, Bardeen and Bublik [29] and others [39,40] showed that Gaussian fluctuations were generic in our observable Universe if a single scalar field interacted through a quartic potential.

In Sec. II, I present the long-wavelength equations for Einstein gravity interacting with scalar fields. In an elegant application of Hamilton-Jacobi theory to general relativity, one may solve this system exactly. Quite remarkably, the full nonlinear dynamics of long-wavelength fields is contained in a single equation, the separated Hamilton-Jacobi equation (SHJE). It is useful for several reasons. The equation is truly covariant in that it makes no reference to either the time parameter nor to the spatial coordinates. When one performs calculations, it is not necessary to make any gauge choice. Exact solutions of the SHJE are given for the case when the scalar fields interact through an exponential potential.

In Sec. III, I describe the initial conditions for the long-wavelength problem. They are determined by short-wavelength quantum fluctuations that began in the Bunch-Davies vacuum [41]. They will be assumed to be Gaussian. In Sec. IV, I consider several models where non-Gaussian fluctuations arise when the scalar fields pass over a strong feature in the potential surface. For multiple scalar fields, the method of calculation is based on some analytic tricks rather than brute-force numerics. Rather than solve the evolution equations through Runge-Kutta integration schemes, I employ Hamilton-Jacobi methods where one introduces new canonical variables.

In Sec. V, I consider the evolution of these fluctuations as they reenter the horizon during the radiation- and matter-dominated eras. In CDM cosmology, non-Gaussian fluctuations may be readily evolved using the transfer function together with a fast-Fourier transform. Contour maps of the density field and the gravitational potential are given at the present epoch.

A summary and a set of conclusions are given in Sec. VI. The models presented may shed some light on the problems of large scale structure in the Universe. Hope-fully, large angle cosmic microwave-background (CMB) anisotropy experiments will provide the most definitive tests of these scenarios.

## II. LONG-WAVELENGTH EQUATIONS FOR SCALAR AND GRAVITATIONAL FIELDS

The inflation scenario will be modeled using Einstein gravity together with $n$ scalar fields $\phi_j$ which self-interact through a potential $V(\phi_j)$. In most models, gravitational radiation is not dynamically important, and I will therefore assume an isotropic metric with inhomogeneous lapse function $N(t,x)$ and scale factor $e^{\alpha(t,x)}$:

$$ds^2 = -N^2(t,x)dt^2 + e^{2\alpha(t,x)}[(dx^1)^2 + (dx^2)^2 + (dx^3)^2].$$

$$(2.1)$$

The inhomogeneous Hubble parameter $H(t,x) \equiv \dot{\alpha}/N$ describes the expansion rate at each point in the Universe. In the long-wavelength approximation, one assumes that the physical wavelengths of all inhomogeneities are larger than the Hubble radius $H^{-1}$. One can then safely neglect all second-order spatial gradients in Einstein's equations, but it is necessary to retain first-order spatial gradients; otherwise the models are homogeneous, and of limited applicability.

Because I wish to employ Hamilton-Jacobi methods, it is useful to define momenta $\pi^\alpha$, $\pi^{\phi_j}$, conjugate to $\alpha(t,x)$ and the scalar fields (Ref. [31], Sec. IV),

$$\dot{\alpha}/N = -\frac{4\pi}{3m_P^2}e^{-3\alpha}\pi^\alpha = H ,$$

$$(2.2a)$$

$$\dot{\phi}_j/N = e^{-3\alpha}\pi^{\phi_j} .$$

$$(2.2b)$$

For each spatial point, the evolution equations [34],

$$\dot{\pi}^{\phi_j}/N = -e^{3\alpha}\frac{\partial V}{\partial \phi_j} ,$$

$$(2.2c)$$

$$\dot{\pi}^\alpha/N = -\frac{4\pi}{m_P^2}e^{-3\alpha}(\pi^\alpha)^2 + \sum_k 3e^{-3\alpha}(\pi^{\phi_k})^2 ,$$

$$(2.2d)$$

and the energy constraint

$$0 = \mathcal{H}(x) = -\frac{2\pi}{3m_P^2}e^{-3\alpha}(\pi^\alpha)^2 + \sum_k \frac{1}{2}e^{-3\alpha}(\pi^{\phi_k})^2$$
$$+ e^{3\alpha}V(\phi_k) ,$$

$$(2.2e)$$

for long-wavelength fields are identical to those of a flat, homogeneous Universe. The new ingredient is the momentum constraint

$$0 = \mathcal{H}_i(x) = -\frac{1}{3}e^{3\alpha}(e^{-3\alpha}\pi^\alpha)_{,i} + \sum_k \pi^{\phi_k}\phi_{k,i} ,$$

$$(2.2f)$$

which connects different spatial points through a first order gradient. (In the above equations, Newton's constant, $G = m_P^{-2}$, is expressed in terms of the Planck scale, $m_P = 1.221 \times 10^{19}$ GeV.)

### A. Hamilton-Jacobi theory for general relativity

In a novel approach to numerical relativity, one may successfully apply Hamilton-Jacobi theory to the solution

of long-wavelength fields [11,12]. I will describe how to solve the long-wavelength cosmological system when the logarithm of the potential is linear. By itself, this system is not sufficient for constructing non-Gaussian models. However, one can construct more complicated potentials by joining several linear $\ln V$ regions together (Secs. III and IV).

I will now give a short review of Hamilton-Jacobi theory for long-wavelength fields. The form of Hamilton's equations is preserved if one employs a generating functional $\mathcal{S}$ to transform the variables $(\alpha(t,x), \pi^{\alpha}(t,x), \phi_j(t,x), \pi^{\phi_j}(t,x))$ to new canonical variables $(\tilde{\phi}_j(t,x), \pi^{\tilde{\phi}_j}(t,x))$:

$$\pi^{\alpha}(t,x) = \frac{\delta\mathcal{S}}{\delta\alpha(t,x)}, \quad \pi^{\phi_j}(t,x) = \frac{\delta\mathcal{S}}{\delta\phi_j(t,x)},$$

$$\pi^{\tilde{\phi}_j}(t,x) = -\frac{\delta\mathcal{S}}{\delta\tilde{\phi}_j(t,x)}. \tag{2.3}$$

There are $2n$ new canonical variables, which is 2 less than

$$-\frac{2\pi}{3m_P^2}e^{-3\alpha(t,x)}\left[\frac{\delta\mathcal{S}}{\delta\alpha(t,x)}\right]^2 + \sum_k \frac{1}{2}e^{-3\alpha(t,x)}\left[\frac{\delta\mathcal{S}}{\delta\phi_k(t,x)}\right]^2 + e^{3\alpha(t,x)}V(\phi(t,x)) \equiv 0. \tag{2.4}$$

As a result, the new variables are independent of time because the Hamiltonian $H_{am} = \int d^3x\, N\mathcal{H}(x)$ generates time evolution through Poisson brackets: i.e.,

$$\dot{\tilde{\phi}}_j = \{\tilde{\phi}_j, H_{am}\} = 0, \quad \dot{\pi}^{\tilde{\phi}_j} = \{\pi^{\tilde{\phi}_j}, H_{am}\} = 0. \tag{2.5}$$

However, the new variables may be spatially dependent: $\tilde{\phi}_j \equiv \tilde{\phi}_j(x)$, $\pi^{\tilde{\phi}_j} \equiv \pi^{\tilde{\phi}_j}(x)$.

Solving the full Hamilton-Jacobi equation, Eq. (2.4) plus second-order spatial gradients, is extremely difficult, and hence one must resort to approximation techniques. The long-wavelength approximation is an elegant extension to inhomogeneous fields of homogeneous minisuperspace. Because there is no causal contact between spatial points, one may write the generating functional as a sum,

$$\mathcal{S} = -\frac{m_P^2}{4\pi}\int d^3x\, e^{3\alpha(t,x)}H(\phi_j(t,x); \tilde{\phi}_j(x)),$$

over the independent evolving spatial points; the Hubble function $H \equiv H(\phi_j; \tilde{\phi}_j)$ has no explicit time or spatial dependence, except through the fields $\phi_j(t,x)$, $\tilde{\phi}_j(x)$.

The long-wavelength equations reduce to

$$H^2 = \frac{m_P^2}{12\pi}\sum_k\left[\frac{\partial H}{\partial\phi_k}\right]^2 + \frac{8\pi V(\phi_k)}{3m_P^2}, \tag{2.6a}$$

$$\sum_k \pi^{\tilde{\phi}_k}\tilde{\phi}_{k,i} = 0, \text{ where } \tilde{\phi}_k \equiv \tilde{\phi}_k(x), \quad \pi^{\tilde{\phi}_k} \equiv \pi^{\tilde{\phi}_k}(x), \tag{2.6b}$$

$$\pi^{\phi_j}(t,x) = -\frac{m_P^2}{4\pi}e^{3\alpha(t,x)}\frac{\partial H}{\partial\phi_j}, \tag{2.6c}$$

the initial number. For general relativity, explicit time dependence of $\mathcal{S}$ is not assumed because one of the field variables becomes the time variable. In this paper, the generating functional $\mathcal{S}$ will depend explicitly on half of the old variables and half of the new ones: $\mathcal{S} \equiv \mathcal{S}(\alpha(t,x), \phi_j(t,x); \tilde{\phi}_j(t,x))$.

Dirac [42] found it useful to introduce the notion of strong and weak constraints. To illustrate the meaning of these expressions, I will consider a trivial example. The function $f(x,y,z) = x^2 + y^2 + z^2 - 1$ vanishes weakly only if the variables $x,y,z$ are constrained to lie on the unit sphere, $x = \sin\theta\cos\phi, y = \sin\theta\sin\phi$, and $z = \cos\theta$, where $\theta,\phi$ are spherical angles. However, the constraint vanishes strongly when expressed in terms of the spherical angles because it yields zero $f(\theta,\phi) \equiv 0$ for all values of $\theta$ and $\phi$. Of course, one has lost one degree of freedom in going from the weak to the strong condition.

In the Hamilton-Jacobi theory for gravity, one insists that the Hamiltonian density, Eq. (2.2e), vanishes strongly when expressed in terms of the new canonical variables:

$$\pi^{\tilde{\phi}_j}(x) = \frac{m_P^2}{4\pi}e^{3\alpha(t,x)}\frac{\partial H}{\partial\tilde{\phi}_j}. \tag{2.6d}$$

The first equation, the separated Hamilton-Jacobi equation (SHJE), is just the energy constraint, whereas the second is the momentum constraint [34]. The last two equations describe how the original variables evolve in a time which can be taken to be $\alpha$ for simplicity.

In essence, a single equation, the SHJE, governs the nonlinear dynamics of the long-wavelength gravitational system. It is remarkable in that it does not refer explicitly either to the time hypersurface nor to the spatial coordinates although it describes both of them. By considering Eqs. (2.2b), (2.2c), and (2.2e), the $n$ evolution equations and the energy constraint for homogeneous minisuperspace are typically written as

$$\frac{1}{N}\frac{\partial}{\partial t}\left[\frac{1}{N}\frac{\partial\phi_j}{\partial t}\right] + 3H\frac{1}{N}\frac{\partial\phi_j}{\partial t} + \frac{\partial V}{\partial\phi_j} = 0, \tag{2.7a}$$

$$H^2 = \frac{8\pi}{3m_P^2}\left[\sum_k\frac{1}{2}\left[\frac{\dot{\phi}_k}{N}\right]^2 + V(\phi_j)\right]. \tag{2.7b}$$

As written, they are difficult to solve because one must make an arbitrary choice of lapse function, and in many cases, one is content to choose a synchronous gauge, $N = 1$. However, the beauty of the Hamilton-Jacobi theory is that one need not make a choice of lapse function. One solves only a single equations rather than $n$ simultaneous ones. In addition, the momentum constraint (2.6b) is easy to solve.

In summary, the long-wavelength problem may be solved by finding a single solution $H \equiv H(\phi_j; \tilde{\phi}_j)$ of the

SHJE, Eq. (2.6a), which depends on $n$ independent parameters $\tilde{\phi}_j$. These parameters are generally spatially dependent, although they are independent of time. Moreover, $n$ additional constants of integration, $\pi^{\tilde{\phi}_j} \equiv \pi^{\tilde{\phi}_j}(x)$, may be found by differentiation of the Hubble function through Eq. (2.6d). The set of parameters $(\tilde{\phi}_j(x), \pi^{\tilde{\phi}_j}(x))$, which are interpreted as new canonical variables, are constrained by the momentum constraint, Eq. (2.6b), which is readily solved. Taking $\alpha$ as time, the evolution of the system $\phi_j \equiv \phi_j(\alpha, \tilde{\phi}_j(x), \pi^{\tilde{\phi}_j}(x))$ is found by inversion of the algebraic equation (2.6d).

### B. Exact solution of the separated Hamilton-Jacobi equation

If the scalar fields interact through a potential whose logarithm is linear [43], one may write down a complete solution of the SHJE [34]. As a result, one may give ana-

lytic expressions for the evolution of the fields $(\phi_1, \phi_2)$ as a function of time $\alpha$. I will be content only to state the results. More details may be found in Ref. [34].

For two scalar fields, consider a potential of the form

$$V(\phi_1, \phi_2; p, \theta)$$

$$= V_0 \exp\left[ -\left[ \frac{16\pi}{p} \right]^{1/2} \frac{(-\phi_1 \sin\theta + \phi_2 \cos\theta)}{m_\mathcal{P}} \right] .$$

$$(2.8)$$

The parameter $p$ controls the steepness of the potential, $\theta$ is the angle between the $\phi_1$ axis and a line of uniform potential, and $V_0$ is the value of the potential at the origin $\phi_1 = \phi_2 = 0$. If $p > 1$, then the potential (2.8) can be used to describe an inflationary epoch. A complete solution of (2.6a) which depends on two arbitrary parameters $b$ and $m$ is

$$H(\phi_1, \phi_2; p, \theta; b, m) = \left[ \frac{8\pi V_0}{3m_\mathcal{P}^2} \right]^{1/2} \left[ \frac{(3p)(m^2+1)}{m^2(3p-1)+3p} \right]^{1/2} \exp\left[ -\left[ \frac{4\pi}{p} \right]^{1/2} \frac{(-\phi_1 \sin\theta + \phi_2 \cos\theta)}{m_\mathcal{P}} \right] \cosh(u) \qquad (2.9a)$$

where $u$ is a function of $b$, $m$, $\phi_1$, and $\phi_2$, which is defined implicitly through

$$\frac{\sqrt{12\pi}}{m_\mathcal{P}} [(\cos\theta - m \sin\theta)\phi_2 - (m \cos\theta + \sin\theta)\phi_1 - b] = -\frac{\sqrt{3p}}{3p-1} [u \sqrt{m^2(3p-1)+3p} + \ln|\cosh(u)|$$

$$- \sinh(u)\sqrt{m^2(3p-1)+3p} |] . \qquad (2.9b)$$

(In the notation of Sec. II $A$, $b = \tilde{\phi}_1$, $m = \tilde{\phi}_2$.) By rotation of fields

$$\phi_1' = \phi_1 \cos\theta + \phi_2 \sin\theta , \quad \phi_1 = \phi_1' \cos\theta - \phi_2' \sin\theta , \qquad (2.10a)$$

$$\phi_2' = -\phi_1 \sin\theta + \phi_2 \cos\theta , \quad \phi_2 = \phi_1' \sin\theta + \phi_2' \cos\theta , \qquad (2.10b)$$

this solution is easily derived from that given by Salopek [34] for scalar fields $(\phi_1', \phi_2')$ whose potential was a function only of the second field $\phi_2'$:

$$V(\phi_1', \phi_2'; p) = V_0 \exp\left[ -\left[ \frac{16\pi}{p} \right]^{1/2} \frac{\phi_2'}{m_\mathcal{P}} \right] . \qquad (2.11)$$

All solutions of the SHJE with potential (2.8) may be derived from Eq. (2.9). Surfaces of constant Hubble parameter are plotted as solid curves in Fig. (1) for the case $m = 1$, $\theta = 0$. The family of orthogonal lines (broken curves) are the physical trajectories. This solution may be verified by differentiation; it is actually derived by looking for symmetries in the SHJE.

Once may invert (2.6c) and (2.6d) to determine the four constants of integration as a function of the original variables $\alpha$, $\phi_j$, $\pi^{\phi_j}$:

$$b \equiv b(\alpha, \phi_j, \pi^{\phi_j}; p, \theta) , \quad \text{and similarly for } m, \pi^b, \pi^m .$$

These complicated analytic expressions are explicitly given in Appendix A [(A1)–(A5)] and they will play a crucial role in what follows.
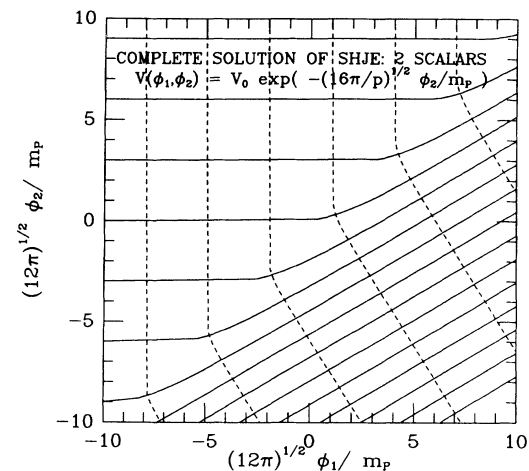


FIG. 1. The complete solution $H(\phi_j; b, m; p, \theta)$ of the separated Hamilton-Jacobi equation is shown for two scalar fields interacting through an exponential potential, Eq. (2.8), with $p = 3$. The broken lines are trajectories of the fields, which are orthogonal to the surfaces of constant Hubble parameter (solid lines). Here, the mixing angle $\theta$ vanishes, and hence surfaces of uniform potential are just horizontal lines. The new canonical variables were chosen to be $b = 0$ and $m = 1$. One can ask what happened to space and time coordinates in the SHJE (2.6a)? Loosely speaking, $\alpha$, the natural log of the scale factor, is the most natural time parametrization of the trajectories. The trajectories themselves represent different spatial points.

### 1. Equation for trajectories in field space

The equation for the trajectories in field space may be explicitly written. It is useful to work in terms of the rotated fields $(\phi_1', \phi_2')$, Eq. (2.10), which are parallel and perpendicular, respectively, to the lines of uniform potential. Given $\phi_1'$, one defines $u$ from which one determines $\phi_2'$:

$$u = u_\infty + \left[\frac{4\pi}{pm_P^2}\right]^{1/2} \sqrt{m^2(3p-1)+3p}\, m^{-1}(\phi_1' - \phi_1'_\infty) \,,$$

(2.12a)

$$\phi_2' = m\phi_1' + b + \frac{m_P}{\sqrt{12\pi}} v(u) \,.$$

(2.12b)

The function $v(u)$ is defined by

$$v(u) \equiv -\frac{\sqrt{3p}}{3p-1}[u\sqrt{m^2(3p-1)+3p} + \ln|\cosh(u)$$
$$- \sinh(u)\sqrt{m^2(3p-1)+3p}\,|] \,, \quad (2.12c)$$

and the constants $\phi_1'_\infty$ and $u_\infty$ are values of $\phi_1'$ and $u$ at $\alpha = \infty$:

$$\phi_1'_\infty = \frac{\pi^m}{\pi^b} + \left[\frac{pm_P^2}{4\pi}\right]^{1/2}\left[\frac{m}{m^2(3p-1)+3p}\right.$$
$$\left. + \frac{m}{\sqrt{m^2(3p-1)+3p}} u_\infty\right] \,,$$

(2.12d)

$$u_\infty = \operatorname{arctanh}\left[\frac{1}{\sqrt{m^2(3p-1)+3p}}\right] \,.$$

(2.12e)

### 2. Late-time evolution of fields

The late-time evolution of the fields during the inflationary epoch determines the initial conditions for structure formation as well as microwave-background fluctuations. As $\alpha \to \infty$, the decaying modes are no longer dynamically important. As can be seen from Fig. (1), $\phi_1'$ approaches $\phi_1'_\infty$, Eq. (2.12d), and $\phi_2'$ evolves according to the attractor solution [34].

$$\ln[\sqrt{\gamma(t,x)}] \equiv 3\alpha(t,x) = 3\sqrt{4\pi p}\,\frac{\phi_2'(t,x)}{m_P} + \zeta(x) \,, \quad (2.13)$$

where $\zeta(x)$ is a constant in time along the trajectory. As a result, $\zeta$ is a function of the new canonical variables:

$$\zeta(x) \equiv \ln|\pi^b| + \tfrac{1}{2}\ln\{(m^2+1)[m^2(3p-1)+3p]\}$$
$$- \frac{\sqrt{36\pi p}}{m_P}\left[1 - \frac{1}{3p}\right](m\phi_1'_\infty + b)$$
$$+ \sqrt{m^2(3p-1)+3p}\, u_\infty - \ln\sqrt{2V_0} \,. \quad (2.14)$$

$\zeta(x)$ gives the variation of the volume element on a time hypersurface of uniform potential, $t = \phi_2'$:

$$\ln[\sqrt{\gamma}(\phi_2',x)/\sqrt{\gamma}(\phi_2',x_0)] = \zeta(x) - \zeta(x_0) \,; \quad (2.15)$$

here, $x$ and $x_0$ are two arbitrary spatial points. $\zeta(x)$, first introduced by Bardeen, Steinhardt, and Turner [44] in linear perturbation theory, is the quantity of primary interest for adiabatic models of structure formation. Please note that the definition (2.13) is 3 times their original definition, $\zeta = 3\zeta_{BST}$. For example, in the CDM model, cosmic microwave-background (CMB) anisotropies at angular scales greater than $\sim 3°$ are proportional to $\zeta$:

$$\Delta T_{CMB}/T_{CMB} \equiv [T_{CMB}(x) - T_{CMB}(x_0)]/T_{CMB}(x_0)$$
$$= -[\zeta(x) - \zeta(x_0)]/15 \,, \quad (2.16)$$

through the Sachs-Wolfe effect (see Sec. V).

### III. INITIAL CONDITIONS

In Sec. IV, models are constructed by joining several linear $\ln V$ potentials together. It will be assumed that Gaussian fluctuations arising from short-wavelength quantum noise are generated in region 1 of the potential which is characterized by parameters $p_1$ and $\theta_1$. A patch of our observable Universe will be described using a finite lattice of spatial points. Non-Gaussian fluctuations in the lattice are produced when one passes over other regions of the potential.

The Hubble function in region 1 of the potential is taken to be the attractor solution

$$H_{att}(\phi_j; p_1, \theta_1) = \left[\frac{8\pi}{3m_P^2}\frac{V_0}{1-1/(3p_1)}\right]^{1/2}\exp\left[-\left[\frac{4\pi}{p_1}\right]^{1/2}\frac{(-\phi_1\sin\theta_1 + \phi_2\cos\theta_1)}{m_P}\right] \,, \quad (3.1)$$

corresponding to the parameters $b = -\infty$ and $m = 0$ in (2.9) having homogeneous values. Given arbitrary initial conditions in region 1, the Hubble parameter will typically relax to such a solution within one expansion time.

In region 1, the fields on the lattice evolve in time $\alpha$ according to Eq. (2.6d):

$$\phi_1(\alpha,x) = -\frac{m_P}{\sqrt{4\pi p_1}}\alpha\sin\theta_1 + \phi_{10}(x) \,,$$
$$\phi_2(\alpha,x) = \frac{m_P}{\sqrt{4\pi p_1}}\alpha\cos\theta_1 + \phi_{20}(x) \,, \quad (3.2a)$$

where $\phi_{i0}(x)$ are the initial values of the scalar fields on a surface where the metric is uniform, $\alpha = 0$. Since I am assuming the attractor solution, the momentum variables are not independent degrees of freedom but are given by partial differentiation of $H_{att}$ through Eq. (2.6c):

$$\pi^{\phi_1}(\alpha,x) = -\frac{m_P}{\sqrt{4\pi p_1}}e^{3\alpha}H_{att}(\phi_j; p_1, \theta_1)\sin\theta_1 \,,$$

$$\pi^{\phi_2}(\alpha,x) = \frac{m_P}{\sqrt{4\pi p_1}}e^{3\alpha}H_{att}(\phi_j; p_1, \theta_1)\cos\theta_1 \,. \quad (3.2b)$$

The new momentum constraint (2.6b) is then satisfied at early times, and the evolution equations guarantee that it will be satisfied at late times.

It is useful to project the initial values of the fields into components parallel and perpendicular to the trajectory:

$$\phi_{10}=\phi_\perp\cos\theta_1-\phi_\parallel\sin\theta_1 \ , \quad \phi_{20}=\phi_\perp\sin\theta_1+\phi_\parallel\cos\theta_1 \ ,$$

$$(3.3)$$

where $\phi_\parallel(x)$ and $\phi_\perp(x)$ are taken to be independent *classical* random fields with a power spectrum:

$$\mathcal{P}_{\phi_\parallel}(k)=\mathcal{P}_{\phi_\perp}(k)\equiv\frac{k^3}{2\pi^2}\langle|\phi_{\parallel,\perp}(k)|^2\rangle \qquad (3.4a)$$

$$=\left[\frac{H_0}{2\pi}\right]^2\left[\frac{k}{H_0e^{\alpha_0}}\right]^{-2/(p_1-1)} . \qquad (3.4b)$$

The power spectrum gives the dispersion in the complex amplitude, $\phi_{\parallel,\perp}(k)$, of a Fourier mode $e^{ik_jx^j}$ with a comoving wave number $k$. It will be assumed that these amplitudes are independent and *Gaussian* distributed. $H_0$ and $e^{\alpha_0}$ are the Hubble parameter and the scale factor, respectively, when the longest mode in the lattice having a physical length $2\pi k_0^{-1}e^{\alpha_0}$ left the horizon, $k_0e^{-\alpha_0}=H_0$. The power spectrum measures the dispersion of the scalar field per $\ln k$ interval. For example, if the discrete Fourier modes in the lattice are approximated by a continuum, then the expectation value for the square of the field in the lattice is

$$\langle\phi_\parallel^2(x)\rangle=\langle\phi_\perp^2(x)\rangle=\int_{H_0e^{\alpha_0}}^\infty\mathcal{P}_{\phi_\parallel}(k)\frac{dk}{k}=\frac{p_1-1}{8\pi^2}H_0^2 \ .$$

$$(3.5)$$

Finite lattice effects alter this formula by factors of order unity. In the actual calculations, the initial conditions are implemented through a fast-Fourier transform. (See Ref. [32] for a more extensive discussion of initial conditions.)

Formula (3.4) assumes that the short-wavelength quantum fluctuations began in the Bunch-Davies vacuum [41,45]. However, as the Universe inflates the wavelength of the fluctuations eventually exceeds the Hubble radius. It is then an excellent approximation to treat the fluctuations using classical random fields in a process termed stochastic inflation [26–33]. In this way, a quantum treatment of the gravitational field is avoided.

The power spectrum Eq. ( 3.4b) decreases with increasing $k$ because the Hubble parameter decreases as the scalar fields roll down the potential in region 1. As a result, quantum noise is no longer significant when $H$ is much smaller than its initial value $H_0$; the subsequent evolution is then governed by the classical long-wavelength equations of Sec. II. In the limit $p_1\to\infty$ one recovers the flat Zeldovich spectrum. However, in practice, one assumes a finite value for $p_1$, which introduces a short-distance cutoff; otherwise Eq. (3.5) would diverge.

The time hypersurface has been chosen to be one of uniform $\alpha$ because in longitudinal gauge the metric fluc-

tuation is small when short-wavelength scalar-field fluctuations leave the horizon [32]. Actually, a better choice of time parameter [32] is $\ln(He^\alpha)$, although for models presented here the improvement is small.

Several conditions must be satisfied in order to justify the initial Gaussian random fields $\phi_{i0}(x)$. Firstly, $H_0$ must be much smaller than the Planck scale $m_\mathcal{P}$ (see Ref. [32]). The potential must also change slowly when the short-wavelength quantum fluctuations on the lattice leave the horizon, i.e., $p_i\gg1$. Both of these conditions are well met in the models of this paper. Lastly, a linear perturbation analysis should be valid for quantum fluctuations with wavelengths smaller than the Hubble radius. This last assumption is questionable since in all inflation models quantum fluctuations start with wavelengths shorter than the Planck length.

In this paper, I have assumed that the energy density of the Universe was once dominated by scalar fields which led to an inflationary epoch. Eventually, the scalar field energy must be transformed into matter and radiation. Because this transition time is not known, the present length scale of the lattice is arbitrary, and it will be assumed to be comparable to that of our observable Universe. The amplitudes of the homogeneous $k=0$ modes are also arbitrary since their dispersion, Eq. (3.4a), is infinite. Finally, $H_0$ is a free parameter whose value is chosen so the resulting fluctuations are large enough to produce structure in our Universe. As a result, the value of the potential at the origin, $V_0$, is irrelevant to the dynamical equations provided that $H_0\gg[8\pi V_0 /3m_\mathcal{P}^2]^{1/2}$. For example, $V_0$ does not enter explicitly in the trajectory equation (2.13).

## IV. MODEL CALCULATIONS

Given an arbitrary scalar field potential $V(\phi_k)$, one could in principle use the evolution equations for homogeneous minisuperspace, Eqs. (2.7a) and (2.7b), to solve the long-wavelength system. In fact, the momentum constraint is satisfied by the initial data of Sec. III, and it is preserved in evolution. However, for the models that produce significant non-Gaussian fluctuations, numerical problems hamper this approach. Typically, two time scales enter, the Hubble time, and another time scale much smaller than it. Hamilton-Jacobi methods thus prove invaluable.

I will consider potentials that are created by joining several linear $\ln V$ potentials together. The interfaces are then straight lines in field space (see Figs. 2 and 3). Fortunately, it is not necessary to perform any numerical integrations. The trajectories in any linear $\ln V$ region have analytic expressions and are characterized by the constants of integration $(b,m,\pi^b,\pi^m)$. By ensuring that the physical fields $(\alpha,\phi_j,\pi^{\phi_j})$ are continuous at the interfaces, one can smoothly match the trajectories from one region to the next. For the models considered, all the field trajectories eventually enter the same linear $\ln V$ region. At late times in the inflationary epoch, one can determine the adiabatic primordial fluctuations for structure formation by calculating the time lag $\Delta\zeta/3=\Delta\alpha$ for different

trajectories to reach the same line of uniform potential.

Three sets of calculations will be given. For illustration purposes, I will first describe a potential consisting of two linear $\ln V$ regions joined at a single interface although it generically produces Gaussian fluctuations. When there are three linear $\ln V$ regions in the potential, then one can indeed generate non-Gaussian fluctuations. When the evolution of the system is viewed in field space, the analysis closely resembles that of geometric optics where one routinely considers a wave front passing over an interface.

### A. Potential with a single interface

In the first instance, consider model $A$ where the potential is obtained by joining two linear $\ln V$ potentials continuously along the line $\phi_2 = \phi_1 \tan \chi_{12}$ [see Fig. 2(a)]. The continuity of the potential, Eq. (2.8), at the boundary implies that the potential parameters $p_2$ and $\theta_2$ in the upper half-plane (region 2) are related to those in the lower half (region 1) through

$$\left[\frac{p_2}{p_1}\right]^{1/2} = \frac{\sin(\chi_{12} - \theta_2)}{\sin(\chi_{12} - \theta_1)} . \tag{4.1}$$

For a given spatial point in the lattice, the value of the fields at the interface follow from the initial conditions in region 1, Eq. (3.2):

$$\alpha_I = \frac{\sqrt{4\pi p_1}}{m_{\mathcal{P}}}[\phi_\perp \tan(\chi_{12} - \theta_1) - \phi_\parallel] , \tag{4.2a}$$

$$\phi_{1I} = \phi_\perp \frac{\cos\chi_{12}}{\cos(\chi_{12} - \theta_1)} , \quad \phi_{2I} = \phi_\perp \frac{\sin\chi_{12}}{\cos(\chi_{12} - \theta_1)} \tag{4.2b}$$

$$\pi_I^{\phi_1} = -\frac{m_{\mathcal{P}}}{\sqrt{4\pi p_1}} H_{\text{att}}(\phi_{jI}; p_1, \theta_1) e^{3\alpha_I} \sin\theta_1 ,$$

$$\pi_I^{\phi_2} = \frac{m_{\mathcal{P}}}{\sqrt{4\pi p_1}} H_{\text{att}}(\phi_{jI}; p_1, \theta_1) e^{3\alpha_I} \cos\theta_1 . \tag{4.2c}$$

Using these values, and assuming that $p = p_2$ and $\theta = \theta_2$, one can determine the constants of integration $(b, m, \pi^b, \pi^m)$, Eqs. (A1)–(A5) in region 2, and then calculate $\zeta$ in region 2 through Eq. (2.14). All the equations are algebraic.

In Fig. 2(a), I display the scalar-field potential as well as some typical trajectories. In Fig. 2(b), I show the distribution of $\zeta$ on a two-dimensional (2D) slice from a $64^3$-lattice calculation. For plotting purposes, the initial value of the Hubble parameter was chosen to be $H_0 = 10^{-2} m_{\mathcal{P}}$, although microwave-background anisotropy limits would require $H_0 < 10^{-4} m_{\mathcal{P}}$. Here, the potential parameters in the lower half-plane are $p_1 = 20$, $\theta_1 = -60°$; in the upper half-plane, $p_2 = 2.7$, $\theta_2 = -30°$. The interface is inclined at an angle of $\chi_{12} = 165°$ to the $\phi_1$ axis. Surprisingly, one still obtains Gaussian statistics Fig. 2(b) although the fields mix at the interface.

In fact, the analytic calculation of $\zeta$ in region 2 is quite straightforward if one neglects homogeneous field (HF) contributions which are uniform over the entire lattice. [Only differences in $\zeta$ are of physical interest; see, for example, Eq. (2.16)]. The new canonical variables in region 2 are [Eqs. (A1)–(A5)]

$$m(x) = \frac{\sin(\theta_1 - \theta_2)}{\cos(\theta_1 - \theta_2) - \sqrt{p_1/p_2}} = \text{HF} , \tag{4.3a}$$

$$b(x) = (\cos\theta_2 - m\sin\theta_2)\phi_{2I}(x) - (m\cos\theta_2 + \sin\theta_2)\phi_{1I}(x) + \text{HF} , \tag{4.3b}$$

$$\ln|\pi^b(x)| = 3\alpha_I(x) - \left[\frac{4\pi}{p_2}\right]^{1/2}[\phi_{2I}(x)\cos\theta_2 - \phi_{1I}(x)\sin\theta_2]/m_{\mathcal{P}} + \text{HF} , \tag{4.3c}$$

$$\pi^m(x)/\pi^b(x) = \phi_{1I}(x)\cos\theta_2 + \phi_{2I}(x)\sin\theta_2 + \text{HF} . \tag{4.3d}$$

Applying Eq. (2.14), $\zeta$ in region 2 admits the simple expression

$$\zeta(x) = 3[\alpha_I(x) - \sqrt{4\pi p_2}(\phi_{2I}(x)\cos\theta_2 - \phi_{1I}(x)\sin\theta_2)/m_{\mathcal{P}}] + \text{HF}$$

$$= 3\sqrt{4\pi p_1}\left[-\frac{\phi_\parallel(x)}{m_{\mathcal{P}}} + \frac{\phi_\perp(x)}{m_{\mathcal{P}}}\tan(\chi_{12} - \theta_1)\left[1 - \frac{p_2}{p_1}\right]\right] + \text{HF} . \tag{4.4}$$

$\zeta(x)$ is a Gaussian random field because it is a linear combination of Gaussian-independent fields $\phi_\parallel(x)$ and $\phi_\perp(x)$. In the continuum limit [see Eq. (3.5)], the standard deviation in $\zeta$ at a single point is readily calculated:

$$\sigma_\zeta \equiv \langle \zeta^2(x)\rangle^{1/2} = 3\sqrt{4\pi p_1}\left[\frac{p_1 - 1}{8\pi^2}\right]^{1/2}\frac{H_0}{m_{\mathcal{P}}}\left[1 + \tan^2(\chi_{12} - \theta_1)\left[1 - \frac{p_2}{p_1}\right]^2\right]^{1/2} , \tag{4.5}$$

which agrees with the numerical results of Fig. 2 if one considers finite lattice corrections. Apparently, each trajectory evolves in a self-similar way. In passing over the interface, $\zeta$ always increases. A simple intuitive derivation of this result based on the attractor approximation will be given in Sec. IV C.

### B. Potential with three interfaces

One can obtain non-Gaussian fluctuations on cosmologically observable scales from a potential created by joining three linear $\ln V$ regions. In order to demonstrate the variety that is possible, I will consider two examples, models B and C, which are illustrated in Figs. 3(a) and 3(b)

Continuity at the various interfaces imply relationships of the potential parameters in addition to Eq. (4.1):

$$\left[\frac{p_3}{p_2}\right]^{1/2} = \frac{\sin(\chi_{23}-\theta_3)}{\sin(\chi_{23}-\theta_2)} , \tag{4.6a}$$

$$\left[\frac{p_1}{p_3}\right]^{1/2} = \frac{\sin(\chi_{31}-\theta_1)}{\sin(\chi_{31}-\theta_3)} . \tag{4.6b}$$

The angles between the interfaces, $\chi_{12}$, $\chi_{23}$, $\chi_{31}$, are not all independent, and one must ensure that

$$1 = \frac{\sin(\chi_{12}-\theta_2)}{\sin(\chi_{12}-\theta_1)}\frac{\sin(\chi_{23}-\theta_3)}{\sin(\chi_{23}-\theta_2)}\frac{\sin(\chi_{31}-\theta_1)}{\sin(\chi_{31}-\theta_3)} , \tag{4.7}$$
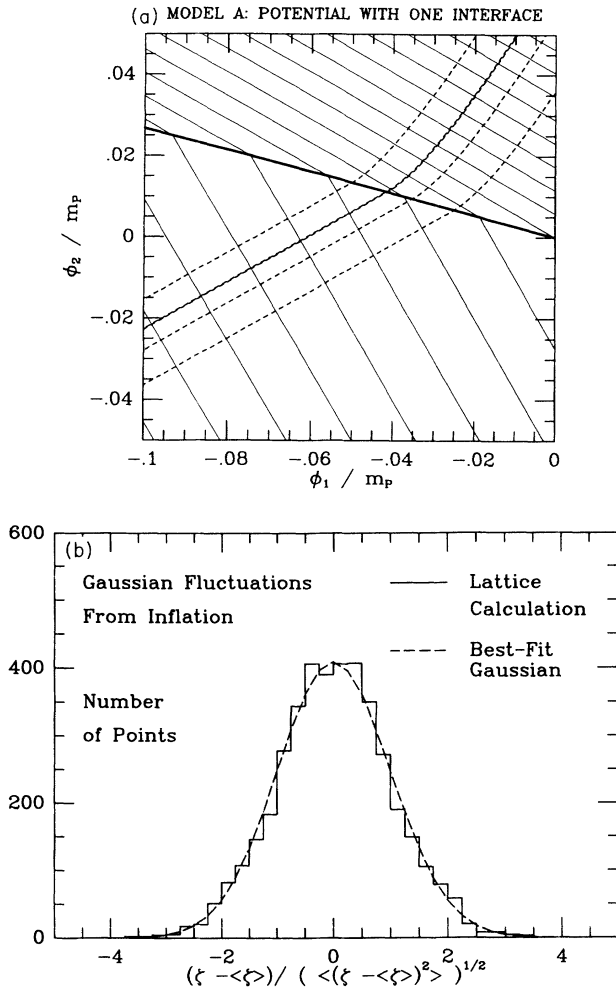


FIG. 2. (a) Some trajectories in field space are shown for a scalar field potential with a single interface between two regions with linear $\ln V(\phi_1,\phi_2)$ (model A). The light solid curves are lines of uniform potential, whereas the very heavy line is the interface. The trajectories (dashed lines) begin in the lower half-plane with Gaussian initial conditions generated from short-wavelength quantum noise. Even when they pass over the interface, the nonlinear metric fluctuation $\zeta$ still remains Gaussian distributed, as shown in the histogram (solid curve) of (b), which compares the results of a $64^3$-lattice simulation with a best-fit Gaussian (dashed curve).
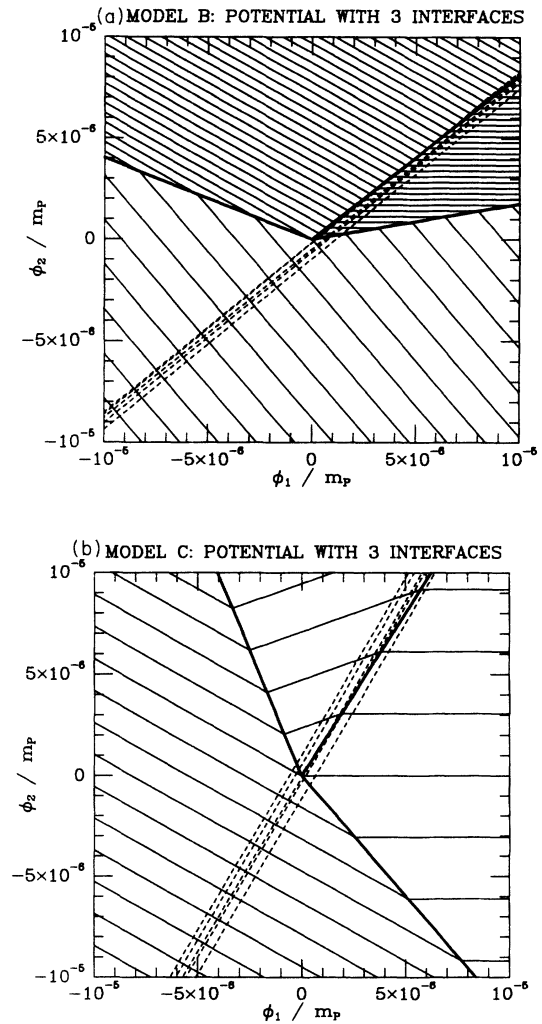


FIG. 3. Non-Gaussian fluctuations consistent with CMB limits may be generated if the scalar fields pass over three interfaces in the potential. Two scalar field potential surfaces, models B and C, displayed in (a) and (b) respectively, are considered in order to illustrate the different geometries that may arise. The light solid curves are lines of uniform potential, whereas the heavy lines are the interfaces. If the scalar field trajectories (dashed lines) pass sufficiently near the origin, nonlinear effects at long wavelengths are important.

which is found by multiplying (4.1) by (4.6a) and (4.6b).

In model B, trajectories begin in the lower half-plane, region 1 ($p_1 = 20$, $\theta_1 = -50°$), with initial Hubble parameter, $H_0 = 10^{-6} m_{\mathcal{P}}$, consistent with CMB limits. If a trajectory enters region 3 (upper left-hand region where $\theta_3 = -30°$), then calculation of $\zeta$ is virtually the same as in Sec. IV A.

However, if the trajectories pass into the upper right-hand area, region 2 ($\theta_2 = 0°$), they receive an upward kick from the potential, which eventually forces them into region 3. (If this diagram were extended, one would find that all trajectories actually cross in region 3.) The angles of the interfaces starting with the lower right and proceeding counterclockwise are $\chi_{12} = 10°$, $\chi_{23} = 39°$, and $\chi_{31} = 158°$. The calculations here are more complicated than those of Sec. IV A because one must determine where a trajectory strikes region 3 after it has passed through region 2. The solution of the intersection point requires the solution of a transcendental equation which may be readily solved if one employs Newton's method. The details are given in Appendix B. Once the fields $(\alpha, \phi_j, \pi^{\phi_j})$ are known at the 2-3 interface, the calculation of $\zeta$ in region 3 proceeds along lines similar to Sec. IV A.

$\zeta$ is not constant in passing through region 2. The evolution of the fluctuations is not adiabatic. In Fig. 4(a), contour maps for $\zeta$ are given for a 2D slice in a $64^3$-lattice calculation of model B. The corresponding distribution of $\zeta$ in region 3 is plotted in Fig. 4(b). For the parameters shown, it was found that non-Gaussian fluctuations can arise if the fields passed sufficiently near the origin, which can be arranged through the choice of the homogeneous mode amplitudes in Eq. (3.3); in fact, the amplitude for the $k = 0$ mode of $\phi_1$ was taken to be $3.9 \times 10^{-7} m_{\mathcal{P}}$. In model B, fluctuations greater than $2\sigma$ have been suppressed, leading to a double peak in the distribution.

The power spectrum for the non-Gaussian field $\zeta$ is shown in Fig. (5). It is found by calculating numerically the dispersion in the Fourier mode amplitudes through Eq. (3.4a). Nonlinear effects do not change the shape of the spectrum which has remained essentially flat. The free parameter $H_0$ sets the amplitude of the fluctuations, which is determined by the galaxy-galaxy correlation function [45].

The length scale associated with the lattice calculation is arbitrary because the fluctuation spectrum is described by a power law. However, if the distance between two adjacent lattice points corresponds to the length subtended by 3° on the surface of last scattering, then Fig. 4(a) may be roughly interpreted as a large-angle microwave-background map. The amplitude of $\langle (\Delta T_{\text{CMB}} / T_{\text{CMB}})^2 \rangle$ is virtually the same as in the CDM case with Gaussian primordial fluctuations. Please note that a large-angle microwave-background map would actually correspond to a spherical shell in the 3D simulation as opposed to a planar slice. In fact, according to Scaramella and Vittorio [46], the histogram Fig. 4(b) will change slightly in going from a planar map to that of a spherical shell. A more careful treatment of microwave-background fluctuations will be considered in the future.

By varying the geometry of the potential surface, one may produce alternative distribution functions. For example, in model C depicted in Fig. 3(b), the potential parameters are chosen so that the scalar fields move more slowly when they cross into region 2 (where $\theta_2 = 0$):


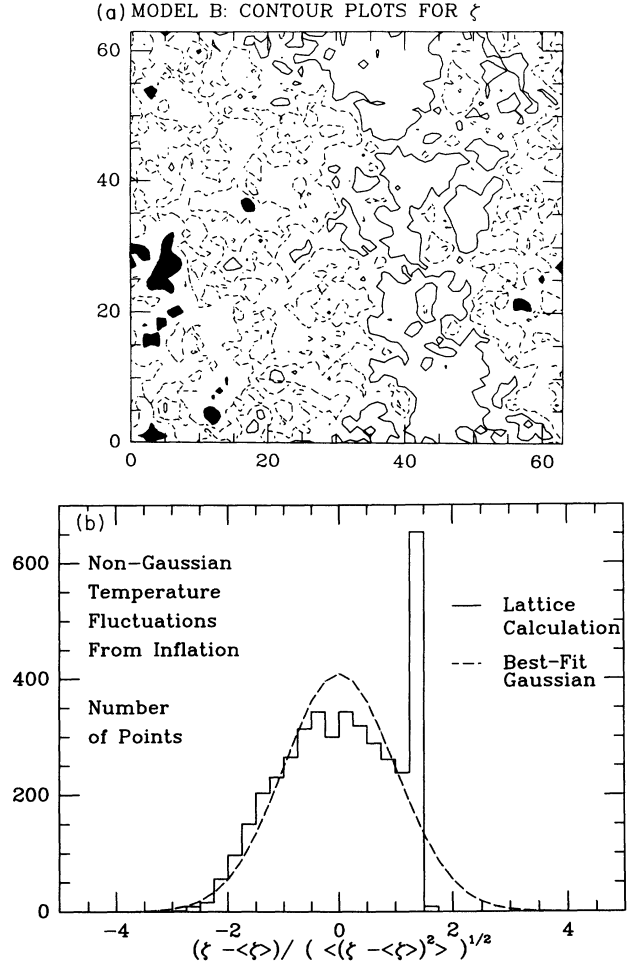
(a) MODEL B: CONTOUR PLOTS FOR $\zeta$



FIG. 4. (a) Contour maps for primordial metric fluctuations $\zeta(x)$ are shown for a 2D slice in a $64^3$-lattice calculation describing model B [Fig. 3(a)]. The dashed lines correspond to $-1\sigma$ and $0\sigma$ fluctuations from the mean of the 2D slice, whereas the solid curve represents a $1\sigma$ deviation. The shaded areas denote regions with fluctuations less than $-2\sigma$. There are no fluctuations from the mean greater than or equal to $2\sigma$. The length scale of the lattice is arbitrary. For example, if the smallest resolvable length scale in the figure, $\frac{1}{64}$ of the lattice size, is chosen to coincide with the angular scale 3°, then this figure is essentially a large-angle microwave-background map, where the temperature anisotropy $\Delta T_{\text{CMB}} / T_{\text{CMB}} = -\Delta \zeta / 15$ is given by the Sachs-Wolfe relation. In (b), the non-Gaussian distribution of $\zeta$ is shown in the 2D slice. For comparison, a Gaussian distribution (dashed curve) with the same mean and dispersion as the histogram is also shown. The most significant feature of these figures is that cold spots in the temperature anisotropy are suppressed over the usual cold-dark-matter (CDM) model with Gaussian primordial fluctuations. The resulting galaxy-formation scenario is interesting because of the presence of sheetlike structures in the evolved density field [see Fig. 9(a)].
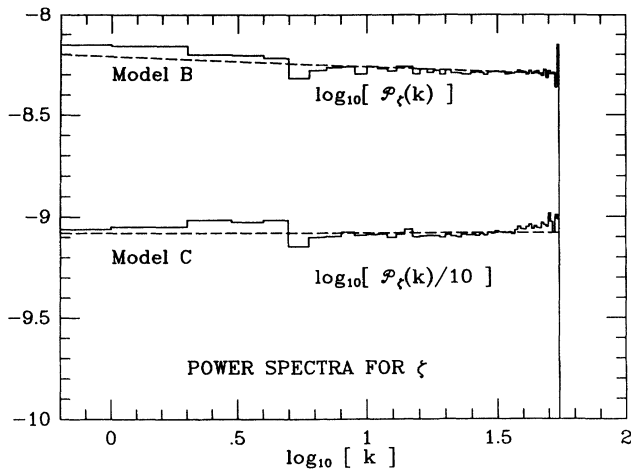
FIG. 5. For both models B and C, the power spectra $\mathcal{P}_\zeta(k) \equiv k^3 \langle |\zeta(k)|^2 \rangle / (2\pi^2)$, for the primordial variable $\zeta$ are calculated by taking the Fourier transform of the $64^3$-lattice simulations described in Figs. 3, 4, and 6. The dashed lines are the best-fit power laws. Nonlinear effects do not change the shape of the flat spectrum whose amplitude is chosen to be approximately $P_\zeta(k) \sim 10^{-8.3}$. The comoving wave number $k = 1$ is the largest mode that can fit in the lattice. The slow monotonic decrease for increasing values of $k$ is a consequence of the Hubble parameter decreasing in region 1 of the scalar-field potential. The larger the potential parameter $p_1$ of region 1 is chosen, the flatter is the fluctuation spectrum. The deviations from a power law seen in the last few bins are not significant because the number of modes within these bins is decreasing, leading to large shot noise.

$\theta_1 = -30°$, $\theta_3 = 20°$; $\chi_{12} = -50°$, $\chi_{23} = 58°$, $\chi_{31} = 112.1°$; $p_1 = 20$, $p_2 = 100.3$, $p_3 = 52.9$. The amplitude for the $k = 0$ mode of $\phi_\perp$ [Eq. (3.3)] was taken to be zero whereas the initial value of the Hubble parameter was $H_0 = 2 \times 10^{-6} m_{\mathcal{P}}$. Contour plots and the associated distribution for $\zeta$ are shown in Figs. 6(a) and 6(b). Model C differs from B in that $-2\sigma$ fluctuations have been clipped from the distribution which exhibits a single sharp peak at $-1\sigma$.

Although the evolution of the fields over the interfaces appears quite complicated, one may find a relatively simple expression for $\zeta$ in terms of $\phi_\parallel$ and $\phi_\perp$. Holding $\phi_\perp$ fixed, one can see that the time lag is simply proportional to $\phi_\parallel$. In fact, one may write $\zeta$ as a sum of the Gaussian random field $\phi_\parallel$ and a function of the independent Gaussian random field $\phi_\perp$:

$$\zeta(x) = -3\sqrt{4\pi p_1} \frac{\phi_\parallel(x)}{m_{\mathcal{P}}} + f(\phi_\perp(x)) . \tag{4.8}$$

The function $f(\phi_\perp)$ can be computed numerically, and it is plotted in Fig. 7. For both models B and C, $f(\phi_\perp)$ is a linear function for $\phi_\perp < 0$ because the corresponding trajectories only pass through two regions; $\zeta$ is then given by a result similar to Eq. (4.4).

However, in model B, $f(\phi_\perp)$ reaches its maximum at the origin, where it has a cusp. In fact, for small positive $\phi_\perp$, $f(\phi_\perp) \propto -\sqrt{\phi_\perp}$. This behavior may be understood qualitatively using a crude analogy. The time for an ob-

ject near the surface of the Earth to fall is also proportional to the square root of its distance if it starts with a negligible vertical velocity. The dominant contribution to $\zeta$ is actually from $f(\phi_\perp)$. The reason that the histogram for $\zeta$ in Fig. 4(b) possesses no $2\sigma$ fluctuations is that the function $f(\phi_\perp)$ reaches its maximum at $\phi_\perp = 0$. By suitable choice of the initial homogeneous values of $\phi_\perp$, one may effectively clip the high $\sigma$ fluctuations. The addition of the term $\propto \phi_\parallel$ in the expression for $\zeta$ serves to convolve the distribution $f(\phi_\perp)$ with a Gaussian random field $\phi_\parallel$.

In model C, $f(\phi_\perp)$ is essentially a linear function for positive values of $\phi_\perp$ although its slope is steeper than
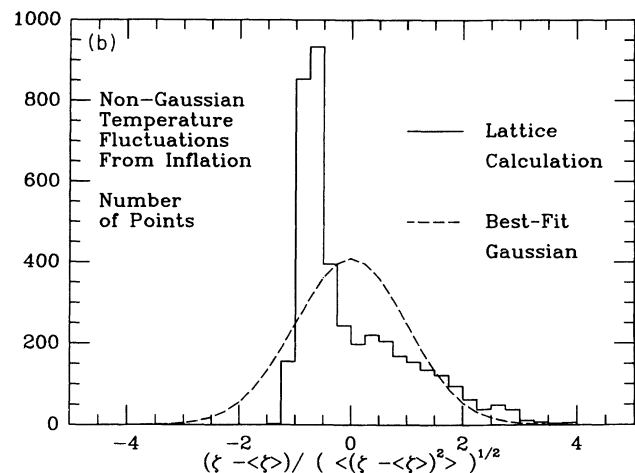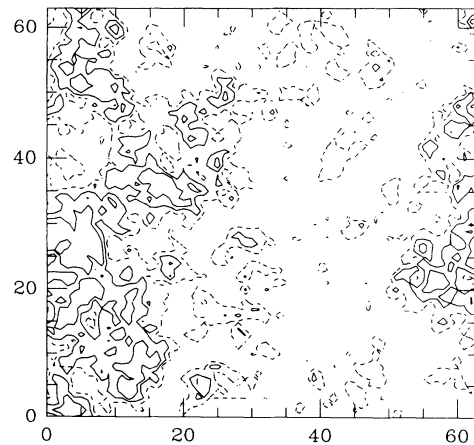


(a) MODEL C: CONTOUR PLOTS FOR $\zeta$



FIG. 6. Same as Fig. 4 except describing model C [Fig. 3(b)]. The broken lines are $-1\sigma$ and $0\sigma$ deviations from the mean of the 2D slice, whereas the solid contours represent $1\sigma$ and $2\sigma$ deviations. However, because of the choice of the scalar field potential, $-2\sigma$ fluctuations in $\zeta(x)$ are absent in this model. Once again, if one identifies the length scales with that of a large-angle microwave-background map, then hot spots in $\Delta T_{CMB}/T_{CMB}$ would be suppressed. In the context of galaxy formation, this model is not appealing because it does not produce more walls or voids than CDM with Gaussian fluctuations [see Fig. 12(a)]. Part (b) gives the distribution of $\zeta$ for the same 2D slice.
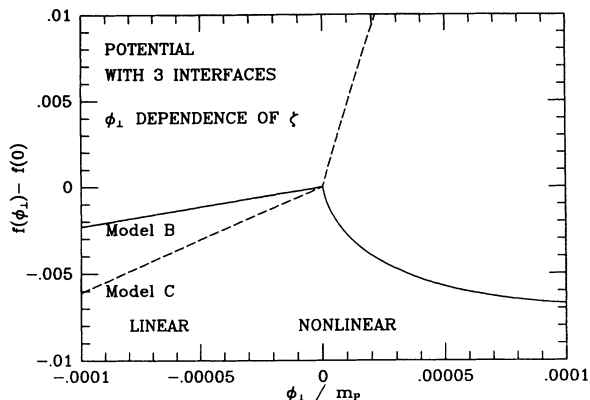
FIG. 7. For scalar field potentials with three interfaces see Fig. 3, $\zeta$ may be written as a Gaussian random field plus $f(\phi_\perp)$, a function of the independent Gaussian random field $\phi_\perp$, Eq. (4.8). Nonlinearities in $f(\phi_\perp)$ are the source of non-Gaussian fluctuations. In model B (solid curve), $f(\phi_\perp)$ reaches its maximum at $\phi_\perp=0$, where there is a cusp. In model C (dashed curve), $f(\phi_\perp)$ is always increasing although there is a kink at the origin. In both cases, $f(\phi_\perp)$ is strongly nonlinear.

that for negative values of $\phi_\perp$. However, there is a kink at the origin which produces non-Gaussian fluctuations.

### C. Analytic calculations based on the attractor solution

Some of the features in the above models may be understood using a simple analytic approximation. After

transients have died away, the fields evolve relatively slowly, and the attractor solution for the Hubble function is an excellent approximation:

$$H_{\text{att}}(\phi_i;p_j,\theta_j)=\left[\frac{8\pi}{3m_{\mathcal{P}}^2(1-1/(3p_j))}V(\phi_i;p_j,\theta_j)\right]^{1/2}.$$

(4.9)

This solution was applied in region 1 of the potential, but now I will consider using it in regions 2 and 3 as well.

In Eq. (4.9), surfaces of uniform potential coincide with uniform Hubble surfaces. The fields move along straight lines orthogonal to these surfaces with uniform speed:

$$v_j\equiv\left[\left[\frac{d\phi_1}{d\alpha}\right]^2+\left[\frac{d\phi_2}{d\alpha}\right]^2\right]^{1/2}=\frac{m_{\mathcal{P}}}{\sqrt{4\pi p_j}}.$$

(4.10)

If the time scale of a variation in the potential is longer than the Hubble time, then the attractor approximation is justified. When the potential changes rapidly, as in the models presented in Secs. IV A and IV B, then one, of course, would expect that the approximation breaks down. However, it still gives surprisingly accurate results in many cases.

For the model A discussed in Sec. IV A, one can apply an analysis similar to that of geometric optics where one calculates phase differences that lead to interference effects. $\Delta\zeta/3$ is just the time lag between two trajectories to reach the same surface of uniform potential (see Fig. 8):

$$\Delta\zeta=3\Delta\alpha=\left[-\frac{\Delta\phi_\|}{v_1}+\frac{d_1}{v_1}-\frac{d_2}{v_2}\right]$$

$$=3\left[-\frac{\sqrt{4\pi p_1}}{m_{\mathcal{P}}}\Delta\phi_\|+\frac{\sqrt{4\pi\rho_1}}{m_{\mathcal{P}}}\Delta\phi_\perp\tan(\chi_{12}-\theta_1)-\frac{\sqrt{4\pi p_2}}{m_{\mathcal{P}}}\Delta\phi_\perp\frac{\sin(\chi_{12}-\theta_2)}{\cos(\chi_{12}-\theta_1)}\right].$$

(4.11)

Once again, $\phi_\perp$ and $\phi_\|$ are the transverse and parallel values of the fields in region 1 (lower half-plane). The distances in the potential surface, $d_1$ and $d_2$, depicted in Fig. 8 result in additional time delays. Applying (4.1), one recovers the previously derived result for $\zeta$, Eq. (4.4), governing a potential with two interfaces. In fact, one could have deduced that transient phenomena would not change the formula for $\zeta$ if one considered the first line of Eq. (4.4).

For potentials obtained by joining three linear $\ln V$ potentials together, the attractor approximation is not as useful, although it does give accurate results when the trajectories are far from the vertex. Geometrically, it should be clear in this instance that for trajectories that enter region 2 and then pass into region 3, the time lag increases linearly with $\phi_\perp$ although the sign may be positive or negative depending on the model considered. Hence, if one considers trajectories that enter and leave the same regions, then the time lag will not introduce non-Gaussian fluctuations from initially Gaussian stochastic noise. Within the context of long-wavelength

fields, it is essential that transient behavior appear, or else some trajectories must pass into different $\ln V$ parts of the potential such as in models B and C.

### D. Length scales with non-Gaussian fluctuations

By definition, for a pure Gaussian random field characterized by a power spectrum, the statistics of the field remain Gaussian no matter what the resolution scale. However, the situation is much more complicated for a non-Gaussian random field. Given the lattice calculation described in Sec. IV B and depicted in Figs. 3–7, I would like to address the question whether a subsample demonstrates non-Gaussian fluctuations. My description will be intuitive.

In this subsection, a probability distribution $Q(\zeta)$ will be considered to be non-Gaussian if for some value of $\zeta$ within two standard deviations of the mean the corresponding value of $Q$ exceeds twice that of a Gaussian distribution: $(2\pi\sigma_\zeta^2)^{-1/2}\exp[-(\zeta-\langle\zeta\rangle)^2/(2\sigma_\zeta^2)]$. This definition is quite arbitrary, but it is sufficient to illustrate
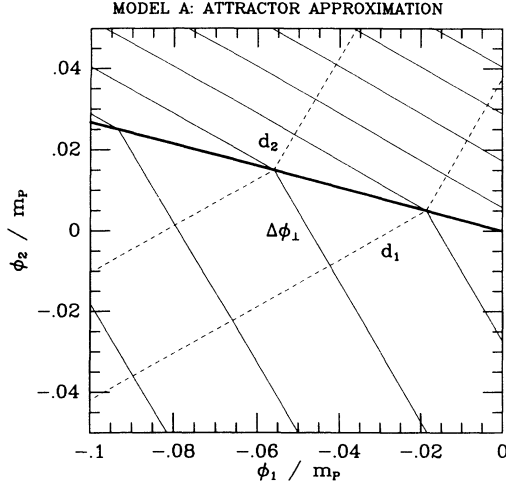
MODEL A: ATTRACTOR APPROXIMATION



FIG. 8. In the attractor approximation, trajectories (dashed lines) in field space move perpendicular to the lines of uniform potential (light solid lines) with constant speed, $v_j \equiv d\phi/d\alpha = m_P/\sqrt{4\pi p_j}$, where $p_j$ describes the steepness of the potential Eq. (2.8) in the $j$th region. The analysis of the resulting metric fluctuations is similar to the calculation of phase differences in geometric optics. $\Delta\zeta/3 = \Delta\alpha$ is just the time lag to reach the same surface of uniform potential. For a potential with a single interface (very heavy line), $\Delta\zeta/3 = d_1/v_1 - d_2/v_2$, where $d_1 = \Delta\phi_\perp \tan(\chi_{12} - \theta_1)$ and $d_2 = \Delta\phi_\perp \sin(\chi_{12} - \theta_2)/\cos (\chi_{12} - \theta_1)$, where $\chi_{12}$, $\theta_1$, $\theta_2$ are the angles associated with the interface, and the lines of uniform potential in the lower and upper half-planes. For simplicity, I have assumed $\Delta\phi_\parallel = 0$. This result agrees with the exact calculation of model A depicted in Fig. 2.

the basic idea.

I will first consider model C. The probability that a subsample, a cube with side $l$, displays non-Gaussian statistics is given approximately by

$$P \approx \frac{1}{\sqrt{2\pi}} \int_{-x}^{x} e^{-t^2/2} dt \ , \quad x = 2 \left[ \frac{l}{l_{max}} \right]^{2/(p_1 - 1)} . \quad (4.12)$$

Here, $l_{max}$ is the length scale associated with the lattice calculations depicted in Figs. 3(b) and Fig. 6(a). As the subsample size decreases to zero, most distributions will be Gaussian. However, fluctuations change from being non-Gaussian to Gaussian when $x \sim 0.2$, and the corresponding length scale is quite small for $p_1 = 20$:

$$\frac{l}{l_{max}} \approx 0.1^{(p_1 - 1)/2} \approx 10^{-10} . \quad (4.13)$$

In model C, if $l_{max}$ corresponds to the size of our observable Universe, the fluctuations in $\zeta$ will be non-Gaussian for almost all length scales of interest to astrophysics. As $p_1$ increases, the power spectrum more closely approximates a flat Zeldovich spectrum, and the transition length scale decreases even further.

The formula is based on some simple considerations of the initially Gaussian field $\phi_\perp$. If the average value of $\phi_\perp$ in a particular cell is denoted by $\bar{\phi}_\perp$, then non-Gaussian fluctuations will typically arise in that cell if the origin $\phi_\perp = 0$ is contained in the $2\sigma$ interval

$(\bar{\phi}_\perp - 2\sigma_{\phi_\perp}(l), \ \bar{\phi}_\perp + 2\sigma_{\phi_\perp}(l))$. The standard deviation $\sigma_{\phi_\perp}(l)$ of a cell with length $l$ contains contributions from wave numbers, $k = (l_{max}/l)H_0 e^{\alpha_0}$ to $k = \infty$, Eq. (3.5):

$$\sigma_{\phi_\perp}^2(l) = \frac{p_1 - 1}{8\pi^2} H_0^2 \left[ \frac{l}{l_{max}} \right]^{2/(p_1 - 1)} . \quad (4.14)$$

In this way, as trajectories associated with the cell roll down the potential, they will straddle the origin where there are strong nonlinearities. Since $\bar{\phi}_\perp$ itself is Gaussian distributed with dispersion given by Eq. (3.5), the fraction of cells in the full lattice which would yield non-Gaussian fluctuations is just the formula (4.12).

In the lattice calculations of model B, the Gaussian distribution for $\bar{\phi}\perp$ is not centered about zero, since the amplitude of $\phi_\perp(k=0)$ was initially taken to be $3.9 \times 10^{-7} m_P$. As a result, Eq. (4.12) for the probability of observing non-Gaussian fluctuations is modified, and it is given approximately by

$$P \approx \frac{1}{\sqrt{2\pi}} \int_{-x-x_0}^{x-x_0} e^{-t^2/2} dt \ ,$$

$$x = 2 \left[ \frac{l}{l_{max}} \right]^{2/(p_1 - 1)} , \quad (4.15)$$

$$x_0 = \phi_\perp(k=0) \bigg/ \left[ \left[ \frac{p_1 - 1}{8\pi^2} \right]^{1/2} H_0 \right] .$$

Once again, if $l_{max}$ is comparable to the size of our observable Universe, the fluctuations are non-Gaussian for those scales of interest for astrophysics.

## V. EVOLUTION OF NON-GAUSSIAN FLUCTUATIONS DURING RADIATION- AND MATTER-DOMINATED ERAS

Although the evolution of the Universe was nonlinear during the inflationary era, the subsequent evolution during the radiation- and matter-dominated epochs may be analyzed using linear perturbation theory, at least until the first formation of stars and galaxies. The evolution is most simply described in Fourier space where the transfer function of each mode has already been computed for adiabatic fluctuations in the CDM model [1]. Calculations evolving non-Gaussian primordial fluctuations are no more difficult than the Gaussian case. For the models considered in Sec. IV, contour plots are given at late times for both the gravitational potential and the density contrast. The prospects of observing non-Gaussian microwave-background fluctuations are discussed. In what follows, I will assume that the present value of the Hubble parameter is $H = 50$ km s$^{-1}$/Mpc.

### A. Cold-dark-matter transfer function

In linear perturbation theory about an Einstein–de Sitter universe, it is still convenient to employ the longitudinal gauge Eq. (2.1) because one may generalize the notion of the Newtonian potential. When the stress perturba-

tions are isotropic, one follows Bardeen [47] in writing the lapse function and the scale factor,

$$N(\tau,x)=a(\tau)[1-\Phi_H(\tau,x)]$$

and

$$e^{\alpha(\tau,x)}=a(\tau)[1+\Phi_H(\tau,x)] \ , \tag{5.1}$$

in terms of the gravitational potential $\Phi_H(\tau,x)$; $\tau$ is conformal time and $a(\tau)$ is the background scale factor. $-\Phi_H$ may be interpreted as the Newtonian potential because it satisfies the Newton-Poisson relation

$$\nabla^2\Phi_H(\tau,x)=-4\pi Ga^2\delta\rho(\tau,x) \ ; \tag{5.2}$$

$\delta\rho(\tau,x)$ is actually the comoving density perturbation, $\rho(\tau,x)-\rho_0(\tau)$, where $\rho_0(\tau)$ is the background density. In Fourier space, this equation is particularly simple:

$$\frac{k^2}{H^2a^2}\Phi_H(\tau,k)=\frac{3}{2}\frac{\delta\rho}{\rho}(\tau,k) \ , \tag{5.3}$$

where the background Hubble parameter is $H=\dot{a}/a^2$ with $\dot{a}$ being the derivative of the scale factor with respect to conformal time. Consistent with current conventions, I use $\Phi_H(\tau,x)$ to denote the gravitational potential in position space, while $\Phi_H(\tau,k)$ will refer to its representation in Fourier space. (For an excellent review of linear perturbation theory, consult Mukhanov *et al.* [48]).

When the wavelength of fluctuations is larger than the Hubble radius, $k/(Ha)\ll1$, the evolution of $\Phi_H(\tau,k)$ is governed by a constant of integration $\zeta(k)$ [44,45]

$$\zeta(k)=\frac{2}{1+p_0/\rho_0}[\Phi_H(\tau,k)+H^{-1}\dot{\Phi}_H(\tau,k)/a]$$
$$+3\Phi_H(\tau,k) \ , \tag{5.4}$$

which measures the metric perturbation on a surface of uniform Hubble parameter. Equation (5.4) relates the Fourier transform of $\zeta(x)$ as defined in Sec. IV [Eq. (2.13)] to the gravitational potential $\Phi_H(\tau,k)$. At all wavelengths, $\Phi_H(\tau,k)$ approaches a constant after the matter-dominated era. Moreover, for those comoving scales that reenter the horizon during that era, the value of $\Phi_H$ at the current epoch $\tau_f$ is given by Eq. (5.4) with $p_0=0$ and $\dot{\Phi}_H=0$:

$$\Phi_H(\tau_f,k)=\zeta(k)/5 \quad [k/a(\tau_f)<0.01 \text{ Mpc}] \ . \tag{5.5}$$

Microwave-background fluctuations smoothed on angular scales larger than 3° are then given by the Sachs-Wolfe formula

$$\Delta T_{\text{CMB}}/T_{\text{CMB}}=-\Delta\Phi_H(\tau_f,x)/3=-\Delta\zeta(x)/15 \ , \tag{5.6}$$

where the functions $\Phi_H$ and $\zeta$ are evaluated on the surface of last scattering. Intuitively, the Sachs-Wolfe result gives the redshift of thermal radiation as it leaves the gravitational potential well; the sign of (5.6) agrees with what one would have naively expected [49].

As defined by Bardeen *et al.* [50], the transfer function $T(k)$ measures the evolution of metric fluctuations after the inflationary epoch. It gives the present value of the

gravitational potential if one knows $\zeta(k)$ from inflation:

$$\Phi_H(k,\tau_f)=T(k)\zeta(k)/5 \ . \tag{5.7}$$

As $k\to0$, $T(k)\to1$, and the result agrees with Eq. (5.5). The transfer function $T(k)$ is real: $T(k)=T^*(k)$. No additional phase factors enter. Given the lattice calculations of Sec. IV, the evolution of $\Phi_H(\tau,x)$ through the linear regime is trivial. One simply Fourier transforms $\zeta(x)$, multiplies each mode by the transfer function $T(k)/5$, and, finally, inverse Fourier transforms the results. In order to obtain $\delta\rho(\tau_f,x)/\rho$ one multiplies $\Phi_H(\tau_f,k)$ by $k^2$ before inverse Fourier transforming [see Eq. (5.3)].

### B. Model distributions at present epoch

Using the non-Gaussian primordial fluctuations of model B described in Fig. 4, contour plots of $\delta\rho(\tau_f,x)/\rho$ are displayed in Fig. 9(a) at the present epoch for a box 128 Mpc to a side. Only $1\sigma$ and $2\sigma$ contours are shown. On the right half of the figure, $2\sigma$ fluctuations are scarce. As a result, the density field is not just a collection of tight sets of islands as one expects for a Gaussian random field. Instead, it appears to be distributed along sheetlike structures. Furthermore, the incorporation of nonlinear evolution would enhance the smooth wall-like features through the Zeldovich pancake mechanism. The corresponding histogram of density fluctuations is plotted in Fig. 9(b). It is mildly non-Gaussian with a peak at $0.8\sigma$. Non-Gaussian fluctuations are more apparent in the gravitational potential given in Figs. 10(a) and 10(b). The broken curves correspond to $-1\sigma$ and $0\sigma$ variations from the mean, whereas the solid curve is a $1\sigma$ variation. There are no $\pm2\sigma$ fluctuations as shown in Fig. 10(b). Particles typically move to the wells of the Newtonian potential, $-\Phi_H$. The resulting pancake structures will not be as lumpy as the case for Gaussian statistics, where the pancakes quickly fragment into clusters. As a result, sheetlike structures are enhanced for the non-Gaussian primordial fluctuations of model B. For the benefit of the reader, the power spectra for $\Phi_H$ and $\delta\rho/\rho$ are displayed in Fig. 11.

Analogously, one may evolve the primordial fluctuations associated with model C. Once again, the $1\sigma$ and $2\sigma$ contours for $\delta\rho(\tau_f,x)/\rho$ at the present epoch are given in Fig. 12(a). These contours are similar to those of a Gaussian random field. However, differences are quite apparent in the histogram of Fig 12(b) which is strongly non-Gaussian. In fact fluctuations less than $-2\sigma$ are highly suppressed. Contour plots for $\Phi_H$ and its distribution are given in Figs. 13(a) and 13(b).

Peebles [13] has proposed that non-Gaussian primordial fluctuations should perhaps be applied in the modeling of structure formation. He has pointed out [14] that the clipping of peaks in the initial *density field* would produce sheet-like features. For example, such structures appear in the slice of the Universe considered by the Center for Astrophysics [3]. Model B presented in this paper also produces smooth sheet-like structures. Basically the result of nonlinear evolution of the scalar fields over the interface is to clip the $2\sigma$ peaks in the *gravita-*

*tional potential* $\Phi_H(\tau,x)$. Since $\delta\rho/\rho$ is related to $\Phi_H$ through the Newton-Poisson relation, it is true in a crude sense that the peaks in $\Phi_H$ correspond to peaks in $\delta\rho/\rho$: one expects high-density fields in the wells of the Newtonian potential $-\Phi_H$. In fact, there are some parts of the lattice where $2\sigma$ peaks in $\delta\rho/\rho$ are nonexistent, although this is not universally true because some $2\sigma$ peaks survive such as in the left half of Fig. 9(a). The signature for non-Gaussian fluctuations is not very pronounced in the histogram for $\delta\rho/\rho$, although it is quite clear in the maps.

By fitting qualitatively the observed distribution of galaxies on the scale of 50 Mpc, model B yields a crude prediction: cold spots in large-angle microwave-background maps should be suppressed as was demon-

strated in Fig. 4. However, this model does not immediately explain the excess power in the galaxy-galaxy correlation function as reported by Maddox *et al.* [5]. Perhaps, it is necessary to incorporate nonlinear evolution of the density field through an *N*-body code.

### C. Prospects for observing non-Gaussian fluctuations

If the microwave-background anisotropy is measured in the near future, then the best test of non-Gaussian fluctuations would come from all-sky maps at large angular scales. For example, if the experimental resolution was $3°\times3°$, one could accumulate approximately 5000 pixel measurements over the entire sky. If experimental systematic effects could be modeled, and if galactic as well as extragalactic radio sources could be removed from the signal, one could then construct a reasonably good histogram of $\Delta T_{CMB}/T_{CMB}$ which could be compared with
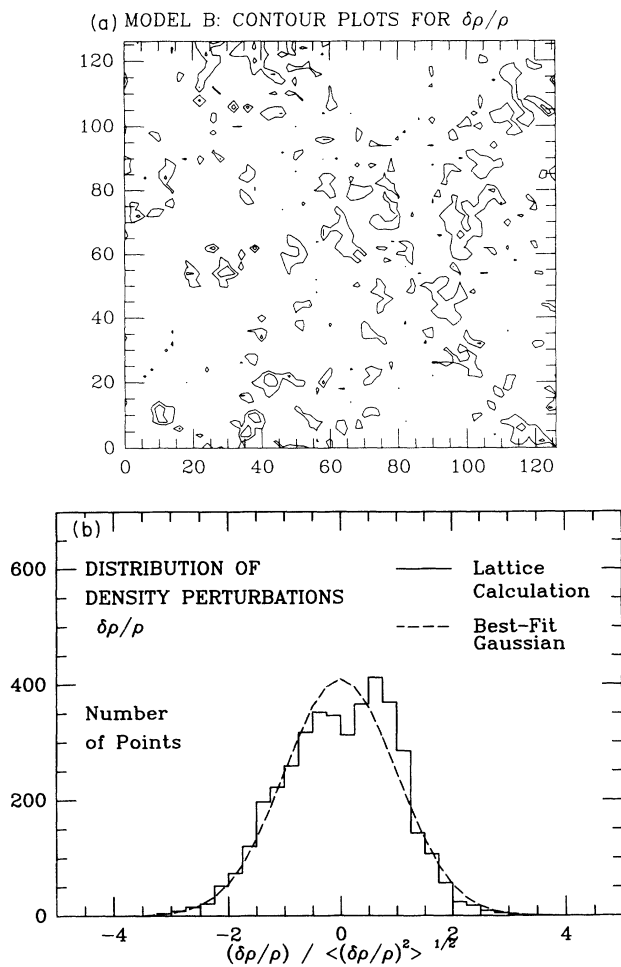


FIG. 9. Evolution of non-Gaussian primordial fluctuations through the radiation- and matter-dominated eras of the CDM scenario is a straightforward application of the transfer function in conjunction with a fast-Fourier transform. In (a) are shown $1\sigma$ and $2\sigma$ fluctuations in $\delta\rho/\rho$ at the present epoch for model B. The box is 128 Mpc wide, assuming that the current Hubble parameter is $H = 50$ km s$^{-1}$/Mpc. In the right half of the box, $2\sigma$ fluctuations are suppressed, thus producing wall-like structures. This scenario is in qualitative agreement with some features of the Center For Astrophysics slice of the Universe. In (b), the histogram for $\delta\rho/\rho$ (solid curve) deviates slightly from a Gaussian (dashed curve).
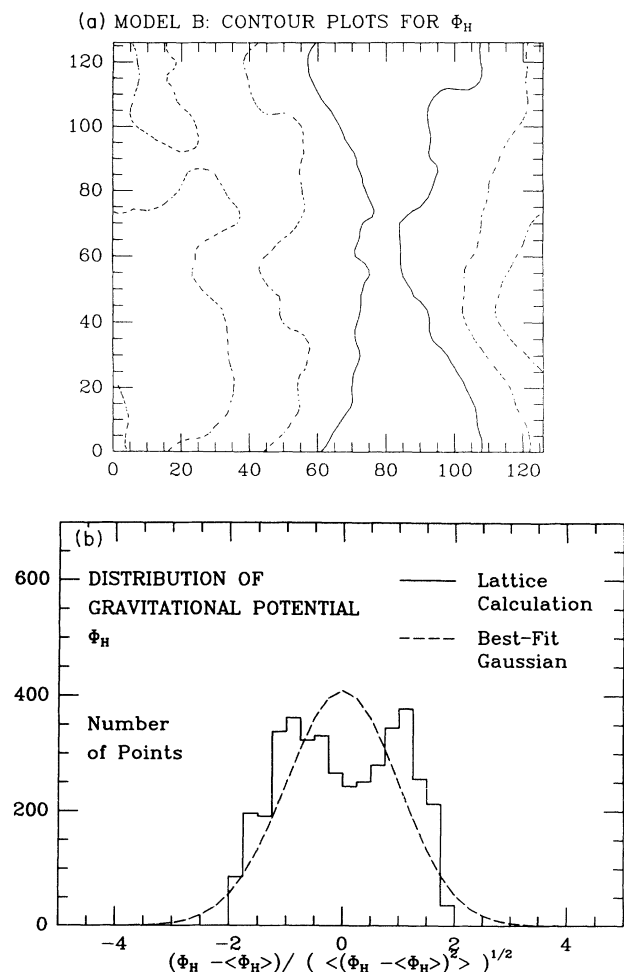


FIG. 10. For model B, contour plots in the gravitational potential $\Phi_H$ are shown at the present epoch for the same slice as Fig. 9(a). The broken curves are $1\sigma$ and $0\sigma$ deviations from the mean of the 2D slice whereas the solid curves are $1\sigma$ fluctuations. There are no $\pm2\sigma$ deviations as can be seen in the histogram of (b). In this model, non-Gaussian fluctutaions are more apparent in the distribution of the gravitational potential than in $\delta\rho/\rho$, Fig. 9(b).
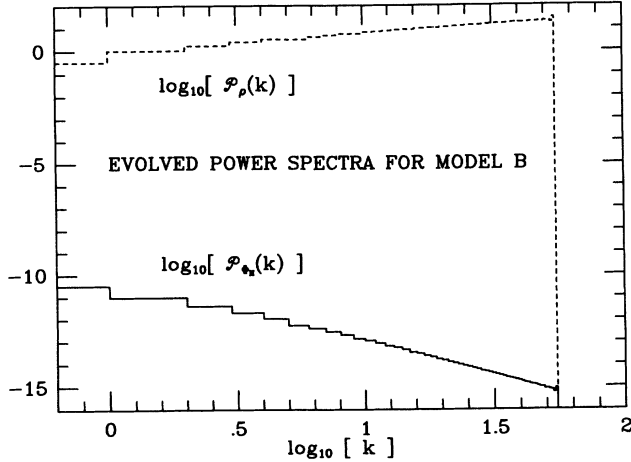
FIG. 11. For model B, the present power spectra in $\Phi_H$ and $\delta\rho/\rho$ (Figs. 9 and 10) are calculated by multiplying the primordial power spectrum in $\zeta$ given in Fig. 5 by the CDM transfer function. $k=1$ corresponds to a wavelength at the present epoch of 128 Mpc. The final shape is essentially the same as CDM with Gaussian statistics. Scale-invariant non-Gaussian fluctuations do not add extra power.

the models of Sec. V B. In the near future, the Cosmic Background Explorer [7] will attempt such maps. In addition, all-sky maps could be provided by balloon-borne experiments [51–53]. Tests at smaller angular scales would probably not give enough independent measurements to test non-Gaussian fluctuations, although the first measurements of anisotropies are indeed likely to come at smaller angular scales [52].

## VI. CONCLUSIONS AND SUMMARY

One can view the phenomenology of large scale structure in the Universe as a three-step process. Firstly, one should construct a viable particle-physics model that is consistent with the required level of metric fluctuations. Embedding inflation in a particle-physics scenario is not easy, although some interesting attempts have been made by Salopek, Bond, and Bardeen [45], as well as Freese, Frieman, and Olinto [54]. Secondly, one should tailor the model to give the correct shape of the fluctuation spectrum. For example, large scale power may be obtained in linear perturbation theory if the scalar-field potential is suitably chosen [45]. However, it is preferable to obtain large-scale power through scales that enter the transfer function (see Bond and Efstathiou [55] who consider the possibility of a decaying 17-keV neutrino). Thirdly, one should ensure that the statistics of the model agree with observations. In this paper, a richer class of inflation models is considered which produce non-Gaussian primordial fluctuations.

The distribution of cosmic microwave temperature anisotropies could serve as a valuable discriminator of various models of the early Universe. For example, it could indicate that nonlinearities in the inflation model were important. It could even determine what was the initial quantum state of the Universe (see, for example, Hartle [56]).

Because the inflation model probes arbitrarily small distance scales, it is quite likely that non-Gaussian fluctuations may arise from the interactions of various fields. However, the greatest obstacle is actually calculating these effects. As the first nontrivial improvement over homogeneous minisuperspace models, one should calculate nonlinear effects at long wavelengths. The long-wavelength system is essentially classical, although short-wavelength quantum noise provides its initial conditions. In addition, it is tractable. By applying analytic solutions for scalar fields self-interacting through an exponential potential, it is not necessary to numerically integrate any differential equations. One can construct viable non-Gaussian models by joining several potential regions where $\ln V(\phi_1, \phi_2)$ is linear. Unfortunately, there is some tuning in the non-Gaussian models of this paper. The initial homogeneous values of the fields are free parameters. If one would change these values, one could produce models that yield only Gaussian fluctuations.
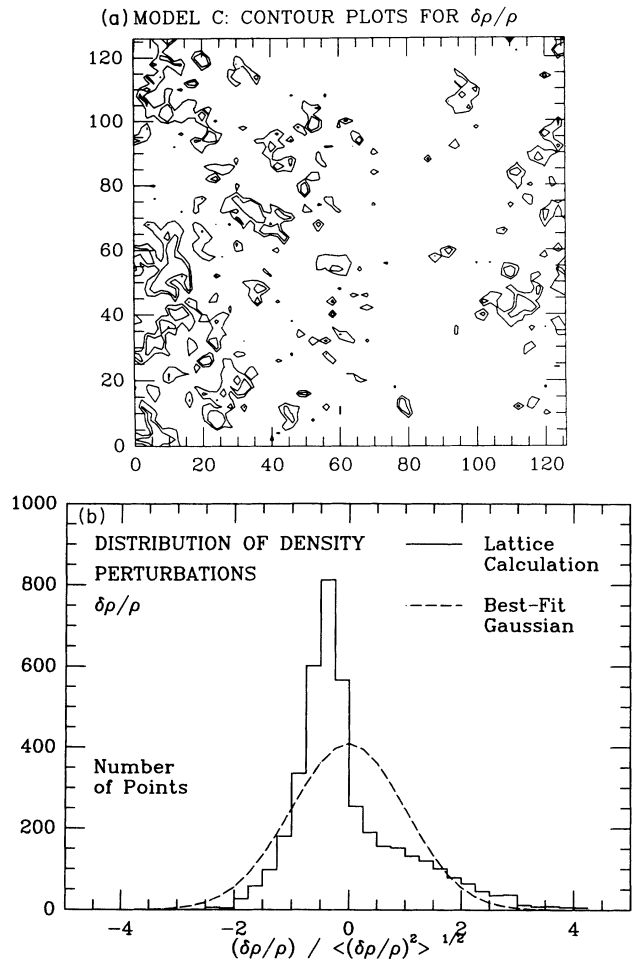




FIG. 12. (a) For completeness, I show the $1\sigma$ and $2\sigma$ contour levels of $\delta\rho/\rho$ for model C at the present epoch. The box has a width of 128 Mpc. Since the $-2\sigma$, $1\sigma$, and $0\sigma$ contours are not drawn, the contour levels shown are somewhat similar to those of CDM with Gaussian fluctuations. Galaxies would presumably correspond to the high-density peaks which appear in tight groups of islands. (b) The histogram of $\delta\rho/\rho$ in the slice is shown; $-2\sigma$ fluctuations are highly suppressed.
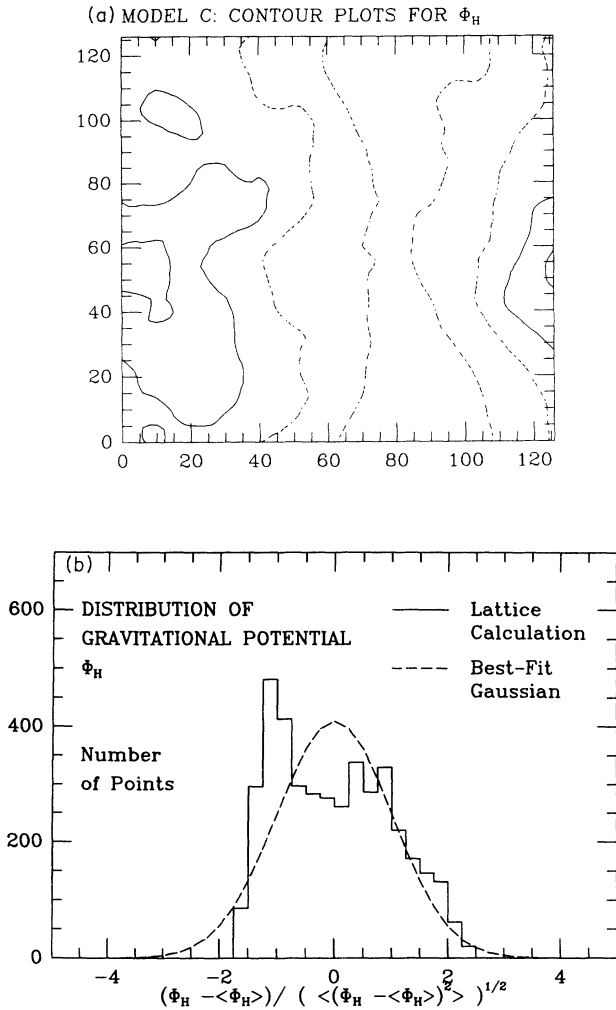
(a) MODEL C: CONTOUR PLOTS FOR $\Phi_H$



(b) DISTRIBUTION OF GRAVITATIONAL POTENTIAL $\Phi_H$ —— Lattice Calculation ---- Best-Fit Gaussian

Number of Points

FIG. 13. For model C, contour plots in $\Phi_H$ are shown in (a) at the present epoch for the same slice as Fig. 12(a). The broken curves are $-1\sigma$ and $0\sigma$ deviations whereas the solid curves are $1\sigma$ and $2\sigma$ fluctuations. There are no $-2\sigma$ deviations, as can be seen in the histogram of (b).

However, the calculation of non-Gaussian fluctuations is only in its infancy, and hopefully more elegant models can be constructed in the future. A scalar field model with many "bumps" in its potential will yield more natural results. In addition, the long-wavelength approximation is only the first step in calculating nonlinearities in inflation models. Richer approximation schemes should be considered in the future.

There is currently no strong cosmological evidence for non-Gaussian fluctuations. One of the goals of the present work was to generate the simple model B that could fit qualitatively the observed sheetlike distribution of galaxies [3]. As a result, one expects that cold spots in the microwave-background maps are suppressed. However, since the primordial fluctuations presented in this paper remain scale invariant, the correlation functions are identical to the CDM case with Gaussian initial conditions. A potential problem with model B is how to account for the excess power in the galaxy-galaxy correlation function as seen by Maddox et al. [5]. The proper interpretation of these observations is being disputed, and perhaps non-Gaussian primordial fluctuations could resolve the discrepancy. For example, it would be interesting to consider $N$-body simulations with the initial conditions from model B.

The definitive test for non-Gaussian fluctuations will hopefully come in the near future from the Cosmic Background Explorer satellite [7] which should be in a position to test the CDM model prediction. In addition, balloon-borne experiments could also provide all-sky microwave-background maps at large angular scales [51–53].

## ACKNOWLEDGMENTS

## APPENDIX A: CONSTANTS OF INTEGRATION FOR COSMOLOGICAL SYSTEMS WITH LINEAR $\ln V(\phi_k)$

For a long-wavelength gravitational system with the potential given by (2.8), there are four constants of integration, the new canonical variables $(b, m, \pi^b, \pi^m)$ which totally characterize the cosmological system. The first two are

$$\pi^b = \pi^{\phi_2}\cos\theta - \pi^{\phi_1}\sin\theta - \frac{1}{\sqrt{3p}}\left\{(\pi^{\phi_1})^2 + (\pi^{\phi_2})^2 + 2e^{6\alpha}V_0\exp\left[-\left[\frac{16\pi}{p}\right]^{1/2}\frac{(\phi_2\cos\theta - \phi_1\sin\theta)}{m_P}\right]\right\}^{1/2}, \tag{A1}$$

$$m = -\frac{\pi^{\phi_1}\cos\theta + \pi^{\phi_2}\sin\theta}{\pi^b}. \tag{A2}$$

It is then convenient to introduce auxiliary fields $u, v$:

$$u = \operatorname{arcsinh}\frac{1}{\sqrt{(3p-1)(m^2+1)}} - \operatorname{arcsinh}v, \tag{A3a}$$

$$v = [2(3p-1)V_0]^{-1/2}\sqrt{m^2(3p-1)+3p}\, m^{-1}e^{-3\alpha}\exp\left[\left[\frac{4\pi}{p}\right]^{1/2}\frac{(\phi_2\cos\theta - \phi_1\sin\theta)}{m_P}\right](\pi^{\phi_1}\cos\theta + \pi^{\phi_2}\sin\theta), \tag{A3b}$$

in which case the remaining new canonical variables are

$$b = (\cos\theta - m\,\sin\theta)\phi_2 - (m\,\cos\theta + \sin\theta)\phi_1$$

$$+ \left[\frac{pm_P^2}{4\pi}\right]^{1/2} \frac{1}{3p-1}[u\sqrt{m^2(3p-1)+3p} + \ln|\cosh(u) - \sinh(u)\sqrt{m^2(3p-1)+3p}\,|\,]\ . \tag{A4}$$

$$\pi^m = \pi^b\left[\phi_1\cos\theta + \phi_2\sin\theta - \left[\frac{pm_P^2}{4\pi}\right]^{1/2}\left\{\frac{m}{m^2(3p-1)+3p} + \frac{mu}{\sqrt{m^2(3p-1)+3p}}\right\}\right]\ . \tag{A5}$$

These expressions were derived in Ref. [34] through differentiation of the Hubble parameter using Eqs. (2.6c), (2.6d), and (2.9).

## APPENDIX B: COMPUTATIONAL NOTES

The calculations described in this paper are purely algebraic. All of the differential equations have been solved analytically, and the numerical methods involve at most the solution of a transcendental equation in a single variable. The most difficult step in the analysis of models B and C in Sec. IV is the determination where the scalar fields strike region 3 in the three interface models. In this appendix, I will describe how to invert the resulting equation.

Given the new canonical variables $(b(x), m(x), \pi^b(x), \pi^m(x))$, Eqs. (A1)–(A5), characterizing a trajectory Eq. (2.12) in region 2, one wishes to find where the scalar fields will intersect the interface with equation $\phi_2 = \phi_1\tan\chi_{23}$. Hence one must solve the following equation for $\phi_1$:

$$\phi_1\tan\chi_{23} = m\phi_1 + b - \frac{m_P}{\sqrt{12\pi}}\frac{\sqrt{3p_2}}{3p_2-1}[u\sqrt{m^2(3p_2-1)+3p_2} + \ln|\cosh(u) - \sinh(u)\sqrt{m^2(3p_2-1)+3p_2}\,|\,]\ , \tag{B1a}$$

where

$$\phi_1 = \phi_{1\,\infty} + \left[\frac{p_2 m_P^2}{4\pi}\right]^{1/2}\frac{m}{\sqrt{m^2(3p_2-1)+3p_2}}(u - u_\infty)\ . \tag{B1b}$$

(Since $\theta_2 = 0$ in region 2, $\phi_1 = \phi_1'$ and $\phi_2 = \phi_2'$.) Before one may proceed further, one needs to know the sign of $\cosh(u) - \sinh(u)\sqrt{m^2(3p_2-1)+3p_2}$. In models B and C, it should be clear that $\phi_1 - \phi_{1\,\infty} < 0$ because $\phi_1$ is initially moving to the right, and hence $\phi_{1\,\infty}$ is the maximum possible displacement of $\phi_1$. Thus, from Eq. (B1b),

$$\mathrm{sgn}[\cosh(u) - \sinh(u)\sqrt{m^2(3p_2-1)+3p_2}] = \mathrm{sgn}[\sinh(u_\infty - u)/\sinh(u_\infty)] = \mathrm{sgn}(m)\ . \tag{B2}$$

After a change of variable and some definitions,

$$z = \exp\beta(\phi_1 - \phi_{1\,\infty})\ , \tag{B3a}$$

where

$$\gamma = 3p_2\left[1 + \left[1 - \frac{1}{3p_2}\right]m\,\tan\chi_{23}\right]\Big/\sqrt{m^2(3p_2-1)+3p_2}\ , \tag{B3b}$$

$$\beta = (\gamma - 1)\left[\frac{4\pi}{p_2 m_P^2}\right]^{1/2}m^{-1}\sqrt{m^2(3p_2-1)+3p_2}\ , \tag{B3c}$$

$$\delta = \frac{\gamma+1}{\gamma-1}\ , \tag{B3d}$$

$$f = -\mathrm{sgn}(m)2\sinh u_\infty \exp\left[\left[\frac{4\pi}{p_2 m_P^2}\right]^{1/2}(3p_2-1)[(m - \tan\chi_{23})\phi_{1\,\infty} + b] - u_\infty\sqrt{m^2(3p_2-1)+3p_2}\right]\ , \tag{B3e}$$

Eq. (B1) may be recast in the more useful form

$$0 = g(z) \equiv z - z^\delta + f\ . \tag{B4}$$

This algebraic equation may be solved using Newton's method (see, for example, Ref. [57]. For the initial guess, one chooses

$$\phi_1 = \frac{\phi_{1I} + \phi_{1\,\infty}}{2}\ . \tag{B5}$$

where $\phi_{1I}$ is the value of the first scalar field at the interface between region 1 and 2. Successive approximations to $z$ are given by

$$z_{j+1} = z_j - g'(z_j)/g(z_j) ,$$

All calculations leading to $\zeta$ are calculated using double precision which is accurate to 15 figures.

After one has determined the value of $\phi_1$ at the 2-3 interface, the corresponding values of $\phi_2$ and $u$ are found from Eq. (2.12). The Hubble parameter $H$ is given by Eq. (2.9a); $\alpha$ is found using Eqs. (A2) and (A3),

$$\alpha = \tfrac{1}{3}\ln\left\{ \frac{\pi^b}{\sinh(u - u_\infty)} \exp\left[ \left[ \frac{4\pi}{p_2} \right]^{1/2} \frac{\phi_2}{m_{\mathcal{P}}} \right] \left[ \frac{m^2(3p_2 - 1) + 3p_2}{2(3p_2 - 1)V_0} \right]^{1/2} \right\} .$$

$\pi^{\phi_1}$ and $\pi^{\phi_2}$ follow from Eqs. (A1) and (A2):

$$\pi^{\phi_1} = -m\,\pi^b ,$$

$$\pi^{\phi_2} = \frac{m_{\mathcal{P}}}{\sqrt{4\pi p_2}} e^{3\alpha}H + \pi^b .$$

Hence, all the field variables $(\alpha, \phi_j, \pi^{\phi_j})$ are known at the interface between regions 2 and 3. One may then determine the new canonical variables $(b, m, \pi^b, \pi^m)$ in region 3 through Eqs. (A1)–(A5) with $\theta = \theta_3$, $p = p_3$. (Note that the field variables are continuous across the interface, but the new canonical variables are not.) Finally, one calculates $\zeta$ in region 3 using Eq. (2.14).

[1] J. R. Bond and G. Efstathiou, Astrophys. J. Lett. **285**, L45 (1984).

[2] N. Bahcall and R. Soneira, Astrophys. J. **270**, 70 (1983).

[3] V. De Lapparent, M. J. Geller, and J. P. Huchra, Astrophys. J. **302**, L1 (1986).

[4] A. Dressler, S. M. Faber, D. Burstein, R. L. Davies, D. Lynden-Bell, R. J. Terlevich, and G. Wegner, Astrophys. J. Lett. **313**, L37 (1986).

[5] S. J. Maddox, G. Efstathiou, W. J. Sutherland, and J. Loveday, Mon. Not. R. Astron. Soc. **242**, 43P (1990).

[6] T. J. Broadhurst, R. S. Ellis, D. C. Koo, and A. S. Szalay, Nature (London) **343**, 726 (1990).

[7] G. F. Smoot et al., Astrophys. J. **371**, L1 (1991).

[8] M. A. Strauss, and M. Davis, Large Scale Structure in the Universe, edited by J. Audouze and A. Szalay, IAU Symposium No. 130 (Reidel, Dordrecht, 1991).

[9] C. S. Frenk, in Proceedings of the NATO Advanced Research Workshop, Durham, England, edited by T. Shanks et al. (Kluwer Academic, Norwell, MA, 1991), p. 355.

[10] N. Kaiser, in Proceedings of the Fourth Canadian Conference on General Relativity and Relativistic Astrophysics, Winnipeg, Canada, edited by G. Kunstatter (World Scientific, Singapore, 1991).

[11] D. S. Salopek, in Proceedings of the NATO Advanced Research Workshop [9], p. 81.

[12] D. S. Salopek, in Proceedings of the Fourth Canadian Conference on General Relativity and Relativistic Astrophysics [10].

[13] P. J. E. Peebles, Astrophys. J. **274**, 1 (1983).

[14] P. J. E. Peebles, Astrophys. J. **317**, 576 (1987).

[15] T. W. B. Kibble, J. Phys. A **9**, 1387 (1976); Y. B. Zeldovich, Mon. Not. R. Astron. Soc. **192**, 663 (1980); A. Vilenkin, Phys. Rev. Lett. **46**, 1169 (1981); N. Turok, Phys. Lett. **126B**, 437 (1983).

[16] A. Albrecht and A. Stebbins, Report No. FERMILAB-PUB-91/17-A, 1991 (unpublished).

[17] H. M. Hodges and J. R. Primack, Phys. Rev. D **43**, 3155 (1991).

[18] C. T. Hill, D. N. Schramm, and J. Fry, Commun. Nucl. Part. Phys. **19**, 25 (1989).

[19] D. La and P. J. Steinhardt, Phys. Lett. B **231**, 231 (1989); E. W. Kolb, D. S. Salopek, and M. S. Turner, Phys. Rev. D **42**, 3925 (1990).

[20] N. Turok, Princeton University Report No. 90-1230, 1990 (unpublished).

[21] T. J. Allen, B. Grinstein, and M. Wise, Phys. Lett. B **197**, 66 (1987).

[22] L. A. Kofman and A. D. Linde, Nucl. Phys. B **282**, 555 (1987); M. Sasaki and J. Yokoyama, Phys. Rev. D **44**, 970 (1991).

[23] J. M. Bardeen, talk presented at the Workshop on Inflation and Exotic Cosmic Structure Formation, Vancouver, Canada, 1990 (unpublished).

[24] J. B. Hartle and S. Hawking, Phys. Rev. D **28**, 2960 (1983).

[25] J. J. Halliwell and S. Hawking, Phys. Rev. D **31**, 1777 (1985).

[26] A. Vilenkin, Phys. Rev. D **27**, 2848 (1983).

[27] A. A. Starobinski, in Field Theory, Quantum Gravity, and Strings, Proceedings of the Seminar, Meudon and Paris, France, 1984–1985, edited by H. T. de Vega and N. Sanchez, Lecture Notes in Physics Vol. 246 (Springer-Verlag, Berlin, 1986), p. 107.

[28] A. D. Linde, Phys. Lett. B **175**, 395 (1986).

[29] J. M. Bardeen and G. J. Bublik, Class. Quantum Grav. **4**, 573 (1987).

[30] A. S. Goncharov, A. D. Linde, and V. F. Mukhanov, Int. J. Mod. Phys. A **2**, 561 (1987).

[31] D. S. Salopek and J. R. Bond, Phys. Rev. D **42**, 3396 (1990).

[32] D. S. Salopek and J. R. Bond, Phys. Rev. D **43**, 1005 (1991).

[33] J. M. Stewart, Class. Quantum Grav. **8**, 909 (1991); B. L. Hu, J. P. Paz, and Y. Zhang, University of Maryland report, 1991 (unpublished).

[34] D. S. Salopek, Phys. Rev. D **43**, 3214 (1991).

[35] A. Ortolan, F. Lucchin, and S. Matarrese, Phys. Rev. D **38**, 465 (1988).

[36] S. Matarrese, A. Ortolan, and F. Lucchin, Phys. Rev. D **40**, 290 (1990).

[37] J. D. Barrow and P. Coles, Mon. Not. R. Astron. Soc. **244**, 188 (1990).

[38] S. Mollerach, S. Matarrese, A. Ortolan, and F. Lucchin, Phys. Rev. D **44**, 1670 (1991).

[39] H. M. Hodges, Phys. Rev. D **39**, 3568 (1989).

[40] I. Yi, E. T. Vishniac, and S. Mineshige, Phys. Rev. D **43**, 362 (1991).

[41] T. S. Bunch and P. C. W. Davies, Proc. R. Soc. London **A360**, 117 (1978).

[42] P. A. M. Dirac, *Lectures on Quantum Mechanics* (Academic, New York, 1965).

[43] F. Lucchin and S. Matarrese, Phys. Rev. D **32**, 1316 (1985); J. J. Halliwell, Phys. Lett. B **185**, 341 (1987); J. D. Barrow, *ibid.* **187**, 12 (1987).

[44] J. M. Bardeen, P. J. Steinhardt, and M. S. Turner, Phys. Rev. D **28**, 679 (1983).

[45] D. S. Salopek, J. R. Bond, and J. M. Bardeen, Phys. Rev. D **40**, 1753 (1989).

[46] R. Scaramella and N. Vittorio, Astrophys. J. **375**, 439 (1991).

[47] J. M. Bardeen, Phys. Rev. D **22**, 1882 (1980).

[48] V. F. Mukhanov, H. A. Feldman, and R. H. Brandenberger, Brown University report, 1991 (unpublished).

[49] P. J. E. Peebles, *The Large Scale Structure of the Universe* (Princeton University Press, Princeton, NJ, 1980).

[50] J. M. Bardeen, J. R. Bond, N. Kaiser, and A. S. Szalay, Astrophys. J. **304**, 15 (1986).

[51] S. P. Boughn, E. S. Cheng, D. A. Cottingham, D. J. Fixsen, and D. T. Wilkinson (unpublished).

[52] P. Meinhold and P. Lubin, Astrophys. J. **370**, L11 (1991).

[53] S. S. Meyer, E. S. Cheng, and L. A. Page, Astrophys. J. **371**, L7 (1991).

[54] K. Freese, J. Frieman, and A. Olinto, Phys. Rev. Lett. **65**, 3233 (1990).

[55] J. R. Bond and G. Efstathiou, CITA report, 1991 (unpublished).

[56] J. B. Hartle, in *Gravitation in Astrophysics (Cargese 1986)*, Proceedings of the NATO Advanced Study Institute, Cargese, France, 1986, edited by J. B. Hartle and B. Carter, NATO ASI Series B: Physics Vol. 156 (Plenum, New York, 1986).

[57] W. H. Press, B. P. Flannery, S. A. Teukolsky, and W. T. Vetterling, *Numerical Recipes* (Cambridge University Press, Cambridge, England, 1986).